MISCELLANEOUS PAPER EL-81-9

ESTUARINE LATERALLY AVERAGED NUMERICAL DYNAMICS

THE DEVELOPMENT AND TESTING OF ESTUARINE BOUNDARY CONDITIONS IN THE LARM CODE

by

John E. Edinger and Edward M. Buchak

J. E. Edinger Associates, Inc.
37 West Ave.
Wayne, Pa. 19087

November 1981

Final Report

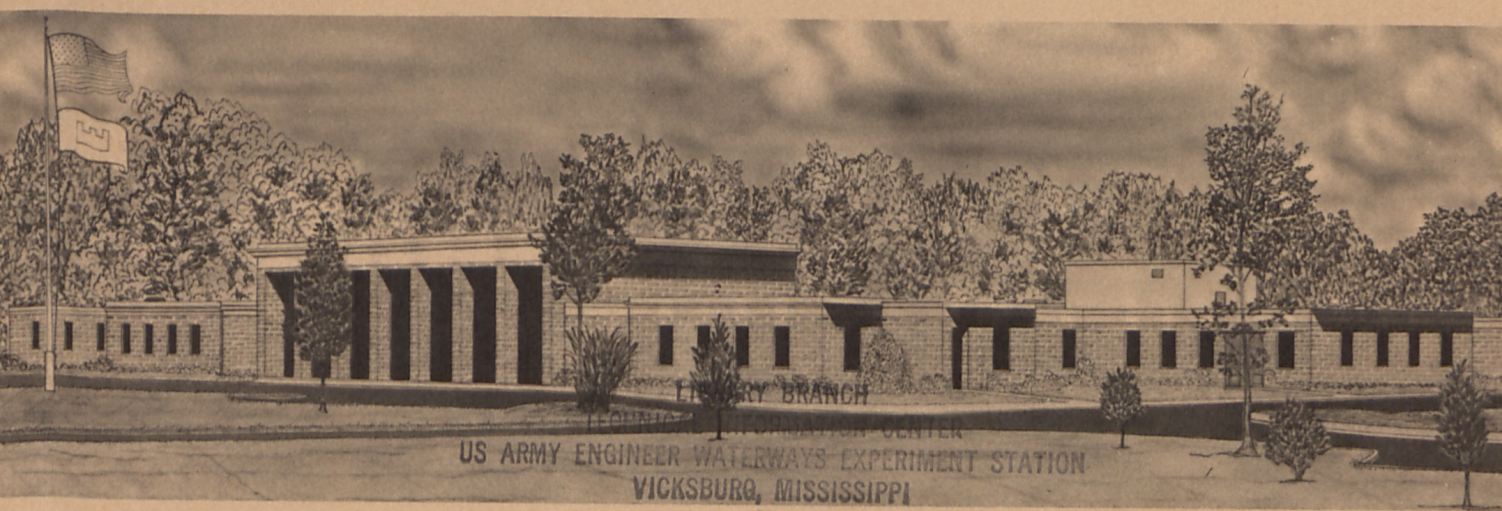

Prepared for Office, Chief of Engineers, U. S. Army, Washington, D. C. 20314

Under Contract No. DACW21-80-C-0042

Monitored by Environmental Laboratory
U. S. Army Engineer Waterways Experiment Station
P. O. Box 631, Vicksburg, Miss. 39180
and
U. S. Army Engineer District, Savannah
P. O. Box 889, Savannah, Ga. 31402

Unclassified

SECURITY CLASSIFICATION OF THIS PAGE (When Data Entered)

REPORT DOCUMENTATION PAGE		READ INSTRUCTIONS BEFORE COMPLETING FORM
1. REPORT NUMBER Miscellaneous Paper EL-81-9	2. GOVT ACCESSION NO.	3. RECIPIENT'S CATALOG NUMBER
4. TITLE (and Subtitle) ESTUARINE LATERALLY AVERAGED NUMERICAL DYNAMICS; THE DEVELOPMENT AND TESTING OF ESTUARINE BOUNDARY CONDITIONS IN THE LARM CODE		5. TYPE OF REPORT & PERIOD COVERED Final report 6. PERFORMING ORG. REPORT NUMBER
7. AUTHOR(s) John E. Edinger Edward M. Buchak		8. CONTRACT OR GRANT NUMBER(s) Contract No. DACW21-80-C-0042
9. PERFORMING ORGANIZATION NAME AND ADDRESS J. E. Edinger Associates, Inc. 37 West Ave. Wayne, Pa. 19087		10. PROGRAM ELEMENT, PROJECT, TASK AREA & WORK UNIT NUMBERS
11. CONTROLLING OFFICE NAME AND ADDRESS Office, Chief of Engineers, U. S. Army Washington, D. C. 20314		12. REPORT DATE November 1981 13. NUMBER OF PAGES 87
14. MONITORING AGENCY NAME & ADDRESS (if different from Controlling Office) U. S. Army Engineer Waterways Experiment Station, Environmental Laboratory, P. O. Box 631, Vicksburg, Miss. 39180 and U. S. Army Engineer District, Savannah, P. O. Box 889, Savannah, Ga. 31402		15. SECURITY CLASS. (of this report) Unclassified 15a. DECLASSIFICATION/DOWNGRADING SCHEDULE

16. DISTRIBUTION STATEMENT (of this Report)

Approved for public release; distribution unlimited.

17. DISTRIBUTION STATEMENT (of the abstract entered in Block 20, if different from Report)

18. SUPPLEMENTARY NOTES

Available from National Technical Information Service, 5285 Port Royal Road, Springfield, Va. 22151.

19. KEY WORDS (Continue on reverse side if necessary and identify by block number)

Computerized simulation
Estuaries
Hydrodynamics
Lakes
Mathematical models
Reservoirs
Water temperature

20. ABSTRACT (Continue on reverse side if necessary and identify by block number)

The longitudinal and vertical hydrodynamics and transport in stratified waterbodies as formulated for the Corps of Engineers Laterally Averaged Reservoir Model (LARM) have been transformed to estuaries by development of appropriate boundary conditions. The resulting computational code Laterally Averaged Estuary Model (LAEM) is tested on the Potomac River estuary for a short period of time with intensive field data.

(Continued)

DD FORM 1 JAN 73 1473 EDITION OF 1 NOV 65 IS OBSOLETE

Unclassified

SECURITY CLASSIFICATION OF THIS PAGE (When Data Entered)

20. ABSTRACT (Continued).

The estuary problem was formulated in terms of spatially varying geometry, a time-varying tide height and salinity distribution at the mouth, and freshwater inflow. The LAEM code was found to reproduce overall estuarine dynamics including tide heights, tide phase shifts, and salinity distributions. In addition, detailed time-varying vertical velocity profiles were produced to a high degree of resolution. Detailed results of the model including the distribution of vertical velocities and turbulent dispersion coefficients were compared to those expected for a coastal plain estuary with favorable agreement.

PREFACE

The work described in this report was conducted by J. E. Edinger Associates for the U. S. Army Engineer District, Savannah (SAS), in partial fulfillment of Contract No. DACW21-80-C-0042. The purpose of the study was to investigate the feasibility of applying the Laterally Averaged Reservoir Model (LARM) with estuarine boundary conditions to narrow, stratified estuaries.

The feasibility study was jointly sponsored by the U. S. Army Engineer Waterways Experiment Station (WES) and the SAS. The WES participation was sponsored by the Office, Chief of Engineers, U. S. Army, under the Environmental Impact Research Program (EIRP).

The study was managed by Mr. Robert Gladden, SAS. Mr. Ross Hall, WES, was the EIRP Principal Investigator. Dr. Billy H. Johnson, Hydraulics Laboratory, WES, provided the technical review. General supervision was provided by Mr. Donald L. Robey, Chief, Ecosystem Research and Simulation Division, WES, and Dr. John Harrison, Chief, Environmental Laboratory, WES. Mr. John Bushman was Technical Monitor for the Office, Chief of Engineers.

Commanders and Directors of WES during the preparation of this report were COL Nelson P. Conover, CE, and COL Tilford C. Creel, CE. Technical Director was Mr. Fred R. Brown.

This report should be cited as follows:

> Edinger, J. E. and Buchak, E. M. 1981. "Estuarine Laterally Averaged Numerical Dynamics; The Development and Testing of Estuarine Boundary Conditions in the LARM Code," Miscellaneous Paper EL-81-9, prepared by J. E. Edinger Associates, Inc., for the U. S. Army Engineer Waterways Experiment Station, CE, Vicksburg, Miss.

CONTENTS

CONVERSION FACTORS, METRIC (SI) TO U. S. CUSTOMARY UNITS OF MEASUREMENT*

Metric (SI) units of measurement used in this report can be converted to U. S. customary units as follows:

Multiply	By	To Obtain
centimetres	0.3937	inches
kilometres	0.5396	miles (U. S. nautical)
metres	3.281	feet

* U. S. nautical miles (nm) are used in this report to describe the study area, define model segment boundaries, and designate the locations where data were collected by the Chesapeake Bay Institute.

ESTUARINE LATERALLY AVERAGED NUMERICAL DYNAMICS; THE DEVELOPMENT AND TESTING OF ESTUARINE BOUNDARY CONDITIONS IN THE LARM CODE

PART I: INTRODUCTION

This report presents the results of a feasibility study of the application of the laterally averaged reservoir model (LARM) with estuarine boundary conditions to the Potomac River estuary. The feasibility study was jointly sponsored by the U. S. Army Engineer Waterways Experiment Station (WES) and the U. S. Army Engineer District, Savannah.

The LARM code was selected for the following reasons:

a. It has been applied successfully to a number of laboratory and reservoir cases over the past three years both within and outside the Corps.

b. The code is quite general for the hydrodynamic equations and can handle features such as layer additions and subtractions and irregular bottom topography.

c. The formulation is spatially implicit and allows for efficiently long computational time steps in deep waterbodies.

d. The code is presently being extended to compute the transport of many interacting water quality constituents through the water quality transport module (WQTM).

Although the LARM code applies to reservoirs, the original basis of the formulations was numerical estuarine dynamics (Edinger, 1974; Edinger and Buchak, 1975).

The Potomac River estuary was selected for the feasibility study because of the availability of pertinent data and existence of comparative numerical model studies. The Potomac is a classical coastal plain estuary exhibiting salinity stratification and baroclinic circulation in the lower reaches. It has detailed geometry data readily available of the type required by LARM (Cronin and Pritchard, 1975). It has been studied in conjunction with various tidal and hydrodynamic models (Rives, 1973; Blumberg, 1975; Elliott, 1976; Wang and Kravitz, 1980). There is a short-term extensive data base of horizontal tidal velocities and salinity collected especially for comparison to models. The Potomac is similar to the James River estuary where Pritchard (1956, 1967) evaluated the distribution of vertical velocity and vertical mixing that can also be compared to model results. The Potomac presents an ideal situation for estuarine model testing and demonstration.

Development of LARM for estuaries began with a re-examination of the implicit numerical formulation of laterally averaged waterbody dynamics and the characteristics of the LARM code. An investigation was made of the dynamics at the downestuary boundary where the velocity profile was computed using the specified tide height and salinity distribution. The only terms relying on auxiliary relationships were the vertical and horizontal dispersion processes. The vertical mixing processes, in particular, are quite important in narrow, deep, and stratified estuaries; hence an extensive investigation was made of their properties for use with LARM.

The model set up and testing included the steps of establishing the model geometry, choosing the numerical boundary and initial conditions, validation, and initial simulations and results. The validation step tested the code with an estuarine boundary for simple cases to assure that there are no computational anomalies. The results of the initial model simulations were summarized and examined using vector plots of the circulation in the estuary throughout a tidal cycle.

The model results were compared to field data for tide height range and phase along the estuary using the data in Rives (1973). The velocity over a number of tidal cycles at different depths and velocity profiles at different times in the tidal cycle were compared to the observations of Elliott and Hendrix (1976). The vertical velocity and dispersion coefficient variations found with the model were compared to the results of Pritchard (1967). These comparisons of model results and field data constitute the model verification. The previous verifications of LARM in reservoirs used only constituent (temperature) distributions because few field measurements existed of the very low velocities found in these waterbodies. The Potomac estuary comparisons are the first velocity verifications of the LARM code.

Numerous features of the model that are not illustrated by the real-time simulations were examined using sensitivity analyses. These included the rate at which salinity becomes distributed throughout the estuary when initialized from zero concentration, the sensitivity of the velocity and salinity profiles to the

vertical dispersion coefficient, and the effects of wind. The latter was examined in detail because wind can be an important force driving estuarine circulation in real situations.

Along with comparing model results and field data to demonstrate model verification, the report elaborates on the important features of estuaries the model describes. The modeling task should eventually be simplified so that the major portion of the effort can be dedicated to assembling and examining the time-varying boundary data and other input data including tide record analysis; boundary salinities; and wind speed, direction, and wave height estimates for dispersion.

The code is recommended for those cases where longitudinal and vertical gradients occur and where lateral homogeneity can be assumed.

PART II: ESTUARINE DYNAMICS IN LARM

The numerical description of estuarine dynamics is formulated from the basic equations of fluid motion. A discussion of the formulation for the laterally averaged, vertically mixed, and sectionally homogenous estuary cases is given in Edinger and Buchak (1980). Details of the laterally averaged relationships are presented here to show the computational basis of the LARM code and its application to estuaries.

The LARM reservoir applications differ from estuary applications only in the specification of boundary conditions. The LARM code also incorporates many computational algorithms such as generalized bottom coordinates, addition and subtraction of top layers, upstream cell addition, and input/output routines that broaden its use in application to estuaries.

The estuarine boundary condition of the varying tide and salinity at the estuary mouth requires that the model compute the fluxes into and out of the estuary from numerical dynamics. Certain approximations are implied in the numerical boundary conditions which may affect results.

Once the hydrodynamics are formulated, there are only two unknown internal parameters. These are the longitudinal and vertical turbulent dispersion parameters. In some estuaries, the latter is more important than the former and more is known about its formulation. These parameters are examined to determine the formulations for use in the estuary version of LARM.

Laterally Averaged Waterbody Dynamics

The laterally averaged equations of fluid motion as they apply to estuaries can be derived from the three-dimensional equations of fluid motion as illustrated in Edinger and Buchak (1980). There are six unknowns and six equations including: (1) the free water surface elevation, η; (2) the pressure, P; (3) the horizontal velocity, U; (4) the vertical velocity, W; (5) the salinity, S; and (6) the density, ρ. The six equations are: (1) the free surface wave equation; (2) the hydrostatic pressure; (3) horizontal momentum; (4) continuity; (5) constituent transport; and (6) an equation of state relating density and salinity.

The laterally averaged equations of fluid motion and transport are the horizontal momentum balance:

$$\frac{\partial UB}{\partial t} + \frac{\partial UUB}{\partial x} + \frac{\partial WUB}{\partial z} = -\frac{1}{\rho}\frac{\partial BP}{\partial x} + \frac{\partial}{\partial x}(BA_x \partial U/\partial x) + \frac{B\partial \tau z}{\partial z} \qquad (1)$$

where B is the estuary width as a function of x and z; and U and W are the laterally averaged horizontal and vertical velocity components. The vertical equation of motion reduces the hydrostatic approximation:

$$\frac{\partial P}{\partial z} = \rho g \qquad (2)$$

The equation of continuity becomes:

$$\frac{\partial UB}{\partial x} + \frac{\partial WB}{\partial z} = qB \qquad (3)$$

where q is the side or tributary inflow per $\Delta x \Delta z B$ volume. Vertically integrated continuity gives the free water surface relationship of

$$\frac{\partial \bar{B}\eta}{\partial t} = \frac{\partial}{\partial x}\int_{\eta}^{h} UBdz - \int_{\eta}^{h} qBdz \qquad (4)$$

where $\bar{B}$ is the time and spatially varing surface width and η is the free water surface elevation. The constituent transport for salt becomes:

$$\frac{\partial BS}{\partial t} + \frac{\partial UBS}{\partial x} + \frac{\partial WBS}{\partial z} - \frac{\partial}{\partial x}(BD_x \partial S/\partial x) - \frac{\partial (BD_z \partial S/\partial z)}{\partial z} = Sq\ B \qquad (5)$$

where Sq is the tributary source flux per $\Delta x \Delta z B$ volume, and

$$\rho = R(S) \qquad (6)$$

is the equation of state. Each additional constituent such as suspended sediment, temperature, or dissolved oxygen has a balance similar to Equation 5 with specific source and sink terms. The equation of state is similarly modified for constituents such as temperature and salinity that have a significant effect on density.

Equations 1 to 6 constitute six equations to be solved for the six unknowns of U, P, W, η, S and ρ. Lateral averaging eliminates the lateral momentum balance, the lateral velocity component, and the Coriolis acceleration. The computational problem is reduced to six equations in six unknowns and, most important, to two coordinate directions. The reduction to two coordinate directions is the main feature that reduces computational time and storage over the three-dimensional case.

The laterally averaged horizontal pressure gradient in the horizontal momentum balance is the density driving force. It can be expanded to

$$\frac{\partial BP}{\partial x} = \frac{B\partial P}{\partial x} + \frac{P\partial B}{\partial x} \tag{7}$$

The second term, $P\partial B/\partial x$, represents the static force of the fluid on the x projection of the lateral boundary which in turn is cancelled by the force of the boundary on the fluid. Thus, $B\partial P/\partial x$ represents the internal fluid horizontal pressure gradient. The horizontal pressure gradient is evaluated from Equation 2 to give

$$B\frac{\partial P}{\partial x} = - \quad gB \frac{\partial \eta}{\partial x} + gB\int_{\eta}^{z} (\partial \rho/\partial x)dz \tag{8}$$

at any depth z. The horizontal pressure gradient is divided into the two components of the surface slope and the vertical integral of the horizontal density gradient. The first term is known as the barotropic gradient and the second as the baroclinic gradient. The horizontal density gradient is the major driving force for the density circulation exhibited in coastal plain estuaries.

The basic characteristics of the longitudinal and vertical free water surface hydrodynamics can be examined through evaluation of the water surface relationship, Equation 4. The vertical integral of the horizontal flow required in Equation 4 can be determined from the algebraic forward time difference of the local acceleration of horizontal momentum in Equation 1. Formulation of the forward time difference of UB is the first step in evaluating the numerical equations. It gives

$$U'B' = UB + gB\Delta t\partial\eta/\partial x - \frac{gB\Delta t}{\rho}\int_{\eta}^{z} (\partial \rho/\partial x)dz + F_x\Delta t \tag{9}$$

where Equation 8 has been substituted for the horizontal pressure gradient and F_x is

$$F_x = \frac{\partial}{\partial x}(BA_x \partial U/\partial x) - \frac{\partial(UUB)}{\partial x} - \frac{\partial WUB}{\partial z} + \frac{\partial B\tau_x}{\partial x} \qquad (10)$$

The vertical integrals of the various terms in Equation 9 can be further evaluated for insertion into the vertical integral of the flow required in the free water surface balance, Equation 4.

The vertical integral of the horizontal pressure gradient can be evaluated from Equation 8 to give

$$\frac{1}{\rho}\int_{\eta}^{h} \frac{B\partial P}{\partial x}\, dz = -\frac{\partial \eta}{\partial x} g \int_{\eta}^{h} B dz + \frac{g}{\rho}\int_{\eta}^{h} \left\{ B \int_{\eta}^{h} \frac{\partial \rho}{\partial x}\, dz \right\} dz \qquad (11)$$

The first term on the right-hand side results from the fact that $\partial \eta / \partial x$ is a function only of x and is constant over z. The integral of width, B, over depth is the total cross-sectional area across which the surface slope contribution to the horizontal pressure gradients acts. The second term is the force due to the horizontal density gradient.

The vertical integral of the horizontal shear stress can be expanded from the derivatives of $\partial B\tau_x/\partial z$ to give

$$\int_{\eta}^{h} \frac{B\partial \tau_x}{\partial z}\, dz = B_h \tau_h - B_\eta \tau_\eta - \int_{\eta}^{h} \tau_x \frac{\partial B}{\partial z}\, dz \qquad (12)$$

The first term is the bottom shear evaluated at z=h and can be evaluated from bottom velocity friction relationships. The surface shear, $B_\eta \tau_\eta$ is the surface wind shear component parallel to the x axis. The third term is the wall or bottom shear due

to the horizontal projection of the sloping sides of the waterbody ($\partial B/\partial z$). It can be evaluated as bottom shear over the projected width ∂B at each elevation. The internal velocity shear cancels out of the vertical integration.

Collecting the various terms of Equation 9 into Equation 4 gives the surface elevation equation of

$$\frac{\partial \bar{B}\eta}{\partial t} - g\Delta t \frac{\partial}{\partial x}\{\frac{\partial \eta}{\partial x}\int_{\eta}^{h} B dz\} = \frac{\partial}{\partial x}\int_{\eta}^{h} U\, B\, dz - \frac{g\Delta t}{\rho}\frac{\partial}{\partial x}\int_{\eta}^{z}\{B\int_{\eta}^{h}\frac{\partial \rho}{\partial x} dz\} dz$$

$$+ \frac{\partial}{\partial x}\{B_h\tau_h - \bar{B}\tau_\eta - \int_{\eta}^{h}\tau_x \frac{\partial B}{\partial z} dz\} \Delta t$$

$$+ \frac{\partial}{\partial x}\{\int_{\eta}^{h} F_x dz\}\Delta t + \{\int_{\eta}^{h} qB\, dz\}\Delta t \qquad (13)$$

With the η or surface coordinate terms collected on the left hand side, Equation 13 is the water surface equation of the integrated waterbody. Equation 13 is, therefore, a numerical form of the frictionally dampened long wave equation for an irregular geometry, stratified waterbody.

For the laterally homogenous estuary, Equation 13 can be simply evaluated implicitly from

$$\frac{-g\Delta t^2}{\Delta x^2}\sigma_{i-1}\eta'_{i-1} + (B_\eta + \frac{g\Delta t^2}{\Delta x^2}\sigma_{i-1} + \sigma_i)\eta'_i \frac{-g\Delta t^2}{\Delta x^2}\sigma_i \eta'_{i+1} =$$

$$B_\eta \eta_i + \Delta t G_i + \Delta t^2 \int_{\eta}^{h} qB dz \qquad (14)$$

Where η'_i is the new time level value of the surface elevation at a finite x location i; σ_i is the total cross-sectional area between i and i+1 locations of η'_i and η'_{i+1}; η_i is the water surface elevation at the previous time step; and G_i is the sum of terms on the right-hand side of Equation 13 except for lateral inflows and outflows. Equation 14 is a spatially implicit surface relationship that eliminates the gravity wave stability criterion. It can be evaluated on each time step using the efficient Thomas algorithm for a tridiagonal martrix. Development and use of Equation 14 in laterally averaged spatially implicit hydrodynamics have been presented in Hamilton (1975) and in Edinger and Buchak (1975, 1980).

The numerical procedure for solving for the six unknowns on each time step is to compute first the water surface elevations from Equation 14 and to obtain the horizontal velocity components from Equation 9. The vertical velocity component is found from continuity, Equation 3, and the salinity distribution from the constituent balance, Equation 5. The water surface elevation equation essentially results from the simultaneous algebraic substitution and solution of horizontal momentum, Equation 1, and vertically integrated continuity, Equation 4, giving U and η simultaneously. This substitution makes the solution spatially implicit in η and U at the same time level, through Equation 14, and eliminates the Courant gravity wave speed criterion that $\Delta x/\Delta t > \sqrt{gH_{max}}$ which leads to short computational Δt in deep waterbodies.

With the laterally averaged equations of motion expressed in an algebraic form, it is necessary to devise a finite difference coding for numerical computations. The coding not only includes the finite difference form of the equations but also the logic and algorithms needed to carry out the computations. These procedures have been developed in the LARM code.

The Numerical LARM Code

The variables are located on a physical space and computational grid as shown in Figure 1. It is called a space staggered grid since certain of the variables are at one location and certain at another. There is a rational basis for choosing the grid locations which can be seen by using imaginary control volumes about a point.

The constituent concentration S is surrounded by a cell that has the U and W at the boundaries. Therefore, the U and W can transport S into and out of this cell with no spatial averaging to determine the change in S over time. Similarly, the W is computed for the same volume using the U's.

The velocity, U, is surrounded by a cell with the water surface elevations, η, and densities known at either end. U is computed from horizontal gradients of the surface slope and density with no spatial averaging of the primary variables. Advection of momentum into and out of the cell does require spatial averaging to determine the fluxes at the ends of the cell, but the variable U being computed remains centered.

The spatial indices of Figure 1 define how the finite differences and integrals in Equations 14, 9, 3, and 5

Figure 1. Estuarine Dynamics from LARM,
Location and Sign Convention for Major Variables

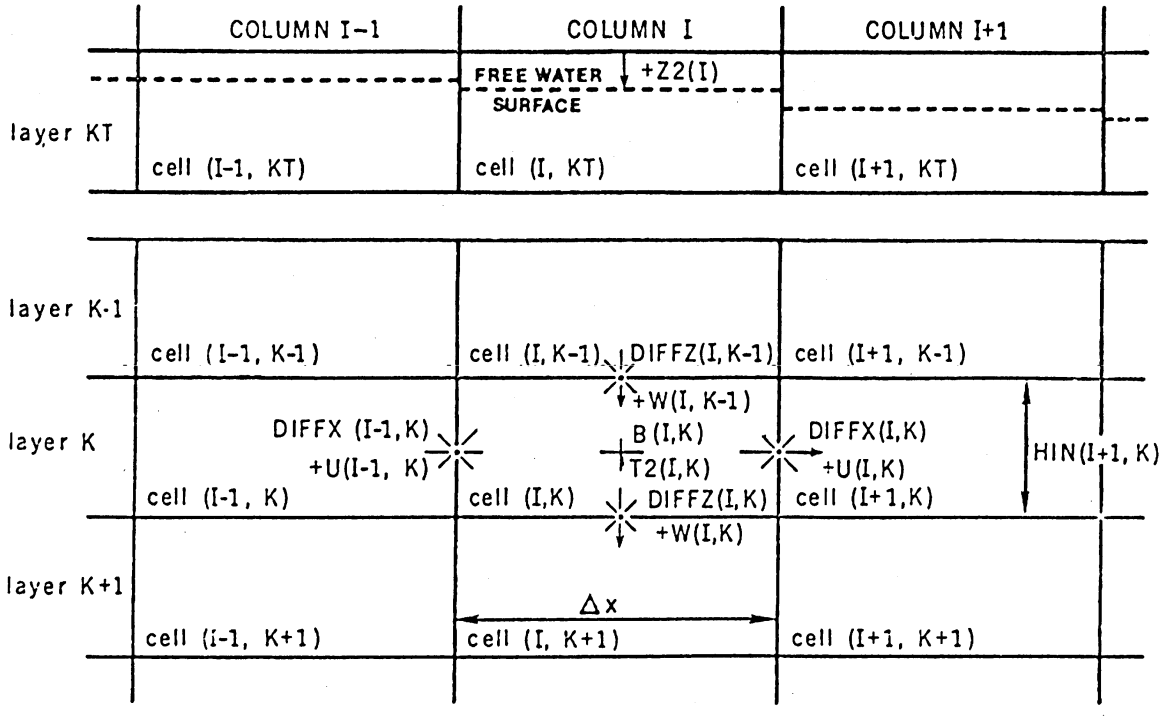

are formed. There is extensive spatial averaging connected with each of the terms in these relationships to account for the spatially varying geometry. This averaging is detailed in Edinger and Buchak (1975, 1980) and need not be expanded on here.

The free water surface elevation, η, varies within the fixed grid in Figure 1. The top layer thickness varies with η and the water surface cannot fall below the computational grid point. When the water surface is rising, it can in principle move up to any elevation and the top layer gets deeper; the computed variables would simply represent lateral averages over the greater depth. Letting the top depth increase without refinement leads to volume errors since width would not change, errors on surface exchange processes, and eventually limited hydrodynamic computations. The problem is severe in reservoirs where water surface elevations can change by 5 to 10 metres,* yet vertical resolution is required to 1 metre. It is particularly important on the Savannah River which has a mean low water depth of about 4 metres and tide of 1 to 2 metres with a spatial resolution required of 0.5 metre. This is the top box problem.

The top box problem has been solved for LARM using a computational algorithm. The procedure is that on a rising water surface, where the elevation in all cells passes a specified level, a new layer is added. Since the variables were computed as laterally homogenous before the new layer, they will then be the value in that layer. On falling water surface where the

* A table of factors for converting metric (SI) units of measurement to U. S. customary units is presented on page 3.

elevation in all cells is below a specified level, then a layer is removed. The logic to carry out this algorithm is quite complex and is incorporated in all steps of the computations.

An important part of the LARM code is the output handling procedures. The basic code outputs grids of the main variables, U, W, S, η at specified times. For reservoir problems, output of results once per day was often satisfactory. Estuaries require at least hourly output and more frequently if tidal average statistics were required. One part of the study has been to develop procedures for retaining results and the routines to perform tidal cycle summaries. It can become very costly to store all the output results for any period of time without the summary routines.

Estuarine Boundary Condition

An estuarine boundary condition specifies tide height (Z_i) and constituent concentrations ($S_{i,k}$, $T_{i,k}$) at the ocean boundary, and computes the boundary fluxes ($U_{i-1,k}$). The basic steps are the computation of the upestuary surface elevations using the specified tide height Z_i in the right-hand boundary side of the surface wave relation, Equation 13, and then computing the boundary $U_{i-1,k}$ from the momentum balance, Equation 9, across the i-1 to i interface.

There are some limitations to the computation of the boundary $U_{i-1,k}$ from the space staggered computational scheme across the boundary. The horizontal momentum computation of $U_{i,k}$ in general depends on (1) the horizontal pressure gradient;

(2) horizontal advection of momentum; (3) vertical advection of momentum; (4) horizontal dispersion of momentum; and (5) vertical dispersion of momentum or interfacial shear as shown in Equation 1. Each term can be examined separately for its evaluation internally and at the boundary to show the limitations of the boundary equations.

The horizontal pressure gradient of the momentum is computed at the boundary similar to the interior points. For the space staggered grid, the horizontal pressure gradient internally falls naturally across the $U_{i-2,k}$ velocity since Z_{i-1} and Z_{i-2} as well as $\rho_{i-1,k}$ and $\rho_{i-2,k}$ are known as are the components of the pressure computation. The same terms are available at the estuary boundary since Z_i and $\rho_{i,k}$ are specified, and Z_{i-1} and $\rho_{i-1,k}$ are computed internally.

The horizontal and vertical advection of momentum in and out of the box require having the advective fluxes with which the centered $U_{i-2,k}$ is transported, and also having the concentration of momentum that is transported. For an interior $U_{i-2,k}$, the horizontal transports are found by averaging. Neglecting geometry changes, the right-hand transport is $(U_{i-2,k} + U_{i-1,k})/2$. This transport can be either out of (+) or into (-) the computational box. When out, it transports $U_{i-2,k}$ and when in, it transports $U_{i-1,k}$. The choice of the quantity being transported from the sign or direction of the advective fluxes is known as upwind differencing. The vertical advection of momentum is similarly treated with the vertical fluxes being averaged as $(W_{i-2,k} + W_{i-1,k})/2$ to be centered at $U_{i-2,k}$ and the momentum transported chosen by the sign of the flux.

Advective fluxes of momentum are not readily evaluated at the estuary boundary. There are no $U_{i,k}$ to the right of Z_i, unless they are specified from data. Similarly, there is no $W_{i,k}$ since there are no $U_{i,k}$ for its determination from continuity.

Horizontal dispersion of momentum is computed for $U_{i-2,k}$ from the horizontal velocity gradient. For an interior point, at $U_{i-2,k}$, the velocities are known for computation of the gradient. For $U_{i-1,k}$, at the estuary boundary there is no known $U_{i,k}$ for the gradient computation. Horizontal dispersion of momentum is not readily included in the boundary computation of $U_{i-1,k}$.

Vertical dispersion of momentum, or vertical shear, is computed from the vertical gradient of $U_{i,k}$ using the vertical profiles of $U_{i,k}$ centered at the bottom of the imaginary computational box. It can be computed at each vertical line of the velocity components including those of the boundary. Bottom shear due to the changing widths in each layer and at the bottom are also readily computed at the boundary.

At the estuarine boundary, the horizontal momentum fluxes are computed from the horizontal pressure gradient, the internal vertical shears, and boundary friction. Neglected by computation with a space staggered grid are the horizontal and vertical advection of momentum and the horizontal dispersion of momentum. There are two possible effects for these computational simplifications. First, the momentum terms neglected in computing the boundary fluxes could become balanced out in the next upestuary

cell which then becomes the real boundary cell. Second, since flux at the boundary is balanced almost solely by internal and bottom friction, the solution near the estuarine boundary could be highly dependent on the vertical momentum dispersion coefficient and the bottom friction factor. These coefficients can be treated locally for the boundary cells as well as upestuary if necessary.

It is expected that there will be some artifical circulation in the first cell upestuary of the boundary due to the lack of momentum transport by advection and dispersion across it. Comparisons of observed and computed velocities upestuary from the boundary will indicate if this circulation has any major effect on the flow field.

Vertical Dispersion Formulations

Vertical dispersion of momentum enters the horizontal momentum balance, Equation 1, through evaluation of the horizontal shear, τ_z. The shear is related to the dispersion process as $\tau_z = A_z \partial U/\partial z$. Vertical turbulent transport of constituent enters the constituent balance, Equation 5, as $D_z \partial S/\partial z$. The terms A_z and D_z are vertical turbulent dispersion coefficients for momentum and constituent, respectively, and are the only terms in laterally averaged numerical relationships that require evaluation.

The source of the turbulent diffusion terms is the temporal averaging that is assumed to apply to the hydrodynamic relationships to give time-smoothed results from fluctuating turbulent flows.

The arithmetic of this step is to represent an instantaneous value of velocity, u, by a short time-averaged mean value U and the fluctuation about the mean, u', as

$$u = U + u' \tag{15}$$

and similarly for the vertical velocity and salinity

$$w = W + w' \tag{16}$$

$$s = S + s' \tag{17}$$

Averaging the vertical advection of momentum term, $\partial\overline{UW}/\partial z$, and the vertical advection of salinity, $\partial\overline{WS}/\partial z$ gives

$$\overline{UW} = U\,W + \langle u'\,w' \rangle \tag{18}$$

and

$$\overline{WS} = W\,S + \langle w'\,s' \rangle \tag{19}$$

where the overbar (—) signifies a time average of the product terms. The momentum and constituent transport balances are for the mean values, U, W, S, and their averaging result in the average cross product fluctuation terms $\langle u'\,w' \rangle$ and $\langle \dot{w}'\,s' \rangle$ which in turn represent the vertical turbulent fluxes of horizontal momentum and salt.

A description of the turbulence processes in a numerical model is complicated by the relationship between the model integration time step, Δt, and the time period of averaging implied in Equation 18 and 19. Presumably, the mean values, U, W, S, are an average over the integration time step and the fluctuations about the mean, u', w', and s', are measured many times within this time step. A short integration time step of a few seconds to one or two minutes approaches the frequency of the fluctuations, yet the model is not actually computing turbulent

fluctuating velocities. Rather, the model is iterating between the time limits of the boundary data to the next solution point. One advantage of an implicit solution with long time steps is that the computed U, W, and S at the end of each time step represents a mean over a period for which the average of the fluctuations apply.

A second difficulty of describing the turbulent transport processes for use in a numerical model is relating them to the scale of the grid. Although the turbulent transport terms are properly multiplied by the width of lateral averaging, the mean velocity and salinity in the gradient terms, $\partial U/\partial z$ and $\partial S/\partial z$, apply across a segment area $B\Delta x$ where B is of the order of hundreds of metres and Δx is of kilometres. The width average is implied when computing U, W, and S but not the length average. Thus, there is a component of spatial variation contained in $\langle u' w' \rangle$ and $\langle w' s' \rangle$, that varies over the computational grid length, Δx.

The average cross product fluctuation terms which make up the vertical turbulent transport process are related to the mean flow and concentration fields predicted by a model as

$$\langle u' w' \rangle = - A_z \partial U/\partial z \qquad (20)$$

$$\langle w' s' \rangle = - D_z \partial S/\partial z \qquad (21)$$

The problem, therefore, reduces to evaluating A_z and D_z in terms of the computed flow and density fields.

In an estuary that can stratify, the vertical dispersion coefficients are affected by the level of turbulence and the degree of stratification. They can be represented as

$$A_z = A_{z_0} F(Ri) \tag{22}$$

where A_{z_0} is a function describing the level of turbulence related to velocity, depth, etc., and Ri is the Richardson number related to stratification. Almost every formulation of A_z that is available can be examined in the form of Equation 22.

The Richardson number is an important concept in describing vertical mixing in a stratified waterbody. It is defined as

$$Ri = \frac{\frac{g}{\rho}\frac{\partial \rho}{\partial z}}{(\frac{\partial U}{\partial z})^2} \tag{23}$$

which is the ratio of the buoyant or potential energy to the kinetic energy being dissipated at a point in the water column. The greater the stratification, as indicated by a large density gradient $\partial\rho/\partial z$, the more a given amount of kinetic energy, $(\partial U/\partial z)^2$, is dissipated by the buoyancy and less by the turbulence generated. An increasing Ri, therefore, means a lower level of turbulence and a lower A_z or D_z. The Ri in Equation 23 is called a "local" Richardson number or gradient Richardson number as opposed to a "bulk" Richardson number applied to the whole water column.

The argument that a high Ri should suppress A_z and D_z and no stratification should have no effect along with some dimensional arguments led Munk and Anderson (1948) to the Richardson number function of

$$F(Ri) = (1 + a\ Ri)^b \tag{24}$$

where they deduced for vertical momentum transport a=10 and b=-1/2 and for density a=10/3 and b=-3/2. Since the exponent,

b, is negative then in Equation 22 a higher Ri leads to a lower A_z. The form of the Richardson number function given in Equation 24 appears in many studies. It tends to have a theoretical basis as shown by the heuristic derivations given by Officer (1976).

Another form of the Richardson number function used by Leendertse and Liu (1975) is

$$F(Ri) = e^{-rRi} \tag{25}$$

which is an exponential form that has a value for negative Ri while Equation 24 can degenerate to zero. A negative Ri exists where an inverse density gradient occurs and mixing takes place by turnover or by vertical convection at a very rapid rate. It can be handled in numerical computations by using an algorithm that sets a large A_z where the density gradient is negative. For large Ri, both Equations 24 and 25 can lead to small A_z, the lower limit of which must be the molecular diffusivity and viscosity.

The most complete evaluation of A_{z_0} and F(Ri) for an estuary has been given by Pritchard (1960). Based on data from the James River and using mixing length arguments, he deduced that

$$F(Ri) = (1 + 0.276\ Ri)^{-2} \tag{26}$$

$$A_{z_0} = 8.59\times10^{-3} U_t \left[z^2(d-z)^2/d^3\right] \tag{27}$$

where U_t is the root-mean-square (RMS) tidal velocity and d is the total depth. The Richardson number was defined as $(g/\rho\ \partial\rho/\partial z)/(0.70U/h)$ where U is the mean velocity over the water column. The function A_{z_0} is shaped to the depth of the water column to be zero at

the surface and bottom and to have a maximum at mid depth based on mixing length arguments. This shape is modified by F(Ri) which because of stratification reduces the mid-depth value. The Ri is computed from a mixture of the local gradient and bulk or water column velocity and depth. It is clearly intended to be a local or depth-dependent evaluation of A_z by choice of the depth function.

The depth-dependent forms of A_z similar to Equations 26 and 27 were tried in numerical models by Bowden and Hamilton (1975) and by Elliott (1976). Both reported numerical instabilities that were apparently related to the evaluation of A_z using a local Richardson number. Bowden and Hamilton (1975) resorted to using a bulk Richardson number but with a vertical shape function. More recently, Bowden (1977) has discussed the difficulties of utilizing the local Richardson number in a numerical model and suggests that there is a theoretical rationale for the bulk Ri. Examination of the numerical form of the Elliott and the Bowden and Hamilton models suggests that the instabilities are a result of computational procedures rather than physical aspects of the mixing problem.

As shown in Part V, LARM is run with a local Ri determined from the local velocity and density gradient using Equation 24. When computations are made for an estuary with a constant A_{z_0}, it produces A_z that has the depth distribution as given by Pritchard (1960). This suggests that the distribution of A_z is a result of the interaction of the mean velocity and salinity fields with the vertical dispersion.

Wind is important in vertical mixing. Wind not only increases the mean velocity gradient and shear, but must also increase the turbulent fluctuations about the mean. It is the fluctuating component over a given period of averaging that determines vertical mixing. Pritchard (1960) assumed that the wind-induced turbulence is proportional to the orbital wave velocity resulting from the wind, and is also affected by the vertical density gradient. The wind speed function deduced by Pritchard (1960) from the James River data is

$$A_{Z_0} = 9.57\times10^{-3} \frac{z(h-z)}{h} \frac{H}{T} e^{-2\pi z/L} \qquad (28)$$

where H is the wind wave height, T is the wave period, L is the wave length, and the resulting A_{Z_0} is additive to Equation 27. In the above relationship, the A_{Z_0} is seen to decrease exponentially with depth and also to have a parabolic shape with depth. The exponential decay is from the wave orbital velocity decay with depth as derived from elementary wave theory. The parabolic shape terms come from the mixing length theory used to scale to the total water column depth. Ford (1976) has examined the wind effects on A_{Z_0} primarily for lakes. The exponential decay is used but there is no shape function with depth. The wind wave characteristics, H, T, and L are functions of wind speed, duration, and fetch. The functional relationships between these variables are known to a limited extent for estuaries. Accurate representation of vertical mixing on estuaries will require performing wind wave analyses at least for significant wind events.

The scale of the computational model grid relative to the waterbody has a significant effect on the magnitude of the dispersion coefficients. Increasing layer thickness from 0.5 m to 1 m and to 2 m reduces the resolution of the computations and the added coarseness may mean larger A_{z_0} if not more uncertain values. In principle, making the grid smaller approaches molecular scales. However, the turbulence in the waterbody consists of random motions and still requires evaluation of the turbulent transport terms <u' w'> and <w' s'> to close the equations of motion and transport for solution. A unique experiment in model scales was to compare LARM computations on a very small grid of Δx=1.52 m and H=7.62 cm to a hydraulic flume with density underflow that was run for obviously laminar conditions (Edinger and Buchak, 1979b). The numerical model did not produce accurate results until the dispersion coefficients were reduced to molecular values, indicating that a strong interrelationship exists between grid size, dispersion coefficients, and turbulent characteristics of the waterbody.

Longitudinal Dispersion Formulations

The longitudinal dispersion of momentum and constituent results from the time averaging that produces the advection of momentum, $\partial UU/\partial x$, in the momentum balance and of constituent, $\partial US/\partial x$, in the transport balance. The average of the product fluctuations about the mean values are for momentum:

$$\langle u' u' \rangle = - A_x \, \partial U/\partial x \qquad (29)$$

and for constituent:

$$\langle u' s' \rangle = - D_x \, \partial S / \partial x \qquad (30)$$

which relates the turbulent fluctuation to the average velocity U and constituent S. As discussed previously, there is a relationship between the time over which the fluctuation products are averaged and the time step of numerical integration that produces U and S.

Most formulations of longitudinal dispersion in estuaries have been derived in relation to one-dimensional sectionally homogenous estuary models. They often come from analysis of steady channel flows and are dimensionally of the form:

$$D_x = a \, h^* u^* \qquad (31)$$

where h* and u* are a characteristic depth and velocity. Harleman (1971) shows that when the Taylor formula is converted from pipe flow to a tidal case, the characteristic velocity translates from the boundary shear velocity to the maximum tidal velocity. Examples of Equation 31 are given in Fischer et al. (1979).

Numerous evaluations of D_x have been made for specific estuaries using a one-dimensional model of the salinity distribution (Officer, 1977). For the Potomac estuary values of 10 to 20 m^2/s were found in the vicinity of Washington, D. C., increasing to 60 m^2/s toward the mouth. Using a dissolved oxygen model on the Delaware, values ranged from 120 to 210 m^2/s over 135 km. The Thames has exhibited values between 50 and 80 m^2/s at low river flows and up to 340 m^2/s at high river flows. The values,

therefore, range from 5 to 500 m^2/s and vary with river flow and salinity stratification. The latter can be complicating since a large D_x required in a one-dimensional model in the stratification region is simply forcing the model to fit a multilayered circulation, and a similarly large D_x would not be required for a laterally averaged model in the same region.

There have been few attempts to derive relationships for the use of A_x and D_x in laterally averaged hydrodynamics except to use relationships of the form in Equation 31 as if they applied to each layer. Experience with LARM has been that two order of magnitude changes in A_x and D_x have not changed results significantly. This insensitivity may be due to upwind differencing. A contributing factor for this lack of sensitivity is that the contribution of vertical exchange to longitudinal mixing which is absorbed in D_x in one-dimensional models is explicitly included in the laterally averaged models. Thus, one of the spatial dimensions over which the turbulent transport is averaged in the one-dimensional model is relaxed in the two-dimensional model and it becomes less important.

There still may be a scale relationship to the grid Δx for A_x and D_x as discussed previously for the flume studies at laminar flow conditions. It suggests that in each computational grid it is necessary to satisfy the condition of

$$Dmol < D_x < U\Delta x \qquad (32)$$

which dimensionally states that constituent (including momentum) should not be diffused out of a cell faster than it is advected

inward. For an estuary like the Potomac where computationally Δx might be 9300 m (5 nautical miles (nm)) and the average net non-tidal velocity is of the order of 0.02 m/s, the above relationship gives 186 m^2/s. The LARM computations use 100 m^2/s; Elliott (1976) used 10^{-4} to 1 m^2/s for similar simulations. There is more to be learned about the role of A_x and D_x in the laterally averaged models as opposed to the one-dimensional cases.

PART III: MODEL SETUP AND TESTING

Setting up the model for a particular estuary requires determining the cross-sectional geometry, describing the boundary conditions and initial conditions, and performing validation computations. After these conditions are established, it is necessary to design simulations that determine how the model performs over a long period of time. Often it is necessary to redesign the simulation conditions in order to compare different results or to obtain different forms of output for post processing.

Model Geometry

The Potomac River estuary is shown in Figure 2. It is 98 nautical miles (nm) from the mouth at Chesapeake Bay to the head of tide. It is 5 to 8 nm wide near the mouth and maintains its breadth to Morgantown near nm 45. For modeling purposes the estuary is conveniently divided into 5-nm segments numbered consecutively from the head of tide to the mouth as shown in Figure 2.

The waterbody geometry in laterally averaged waterbody dynamics is represented by the width of the waterbody at each depth at the center of each computational cell. Cross-sectional geometry of the Potomac River estuary is tabulated for every nautical mile in Cronin and Pritchard (1975). Estuarine widths for the Potomac used in the model are given in Table 1. Table 1 also shows the computational scheme of the model as the combination of I's and K's that make up the computational grid.

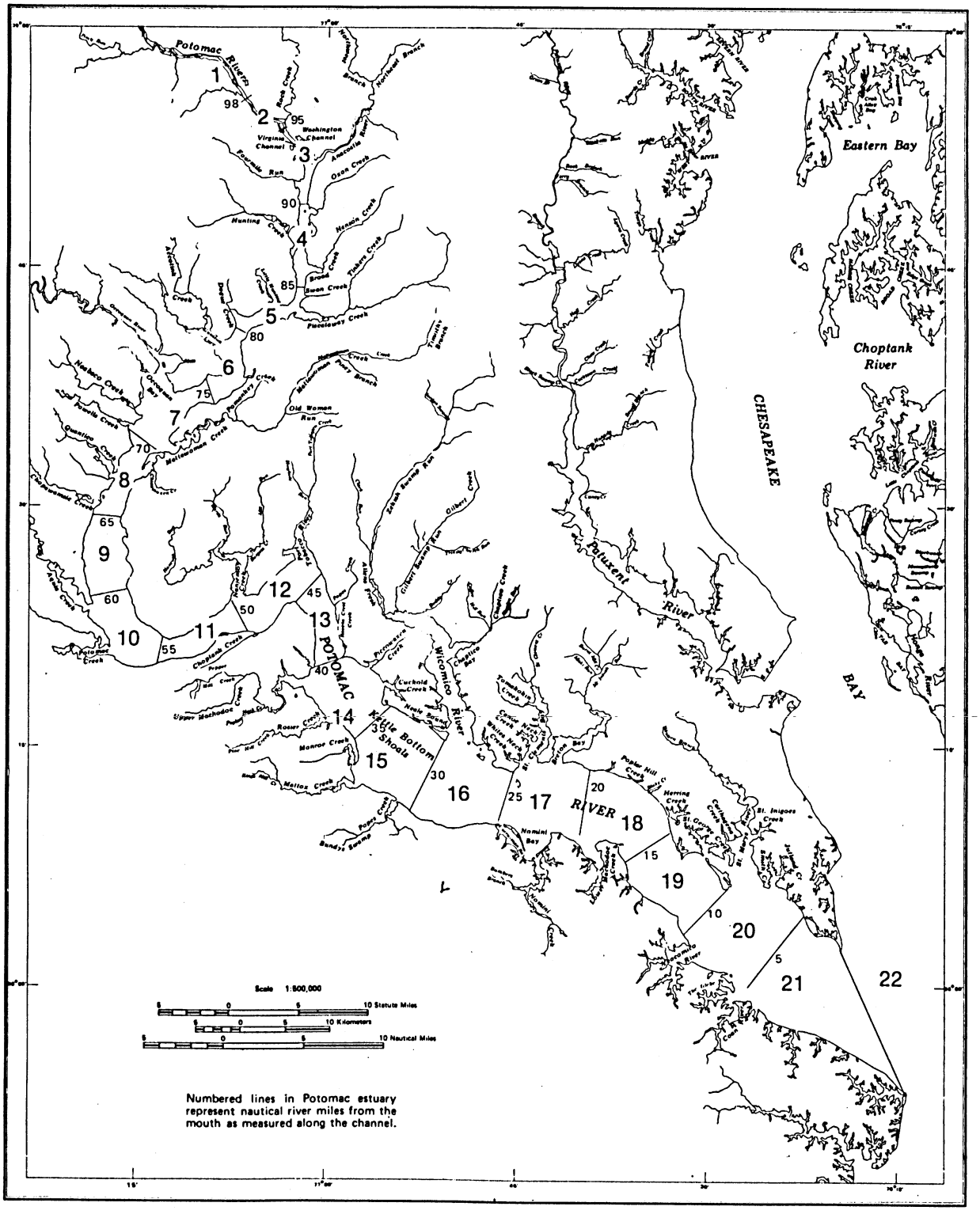

Figure 2. Potomac River Estuary

The scheme is 20 segments long of 5 nm each and up to 11 layers deep each of 2 metres. The shallow reach from model segment 15 to 17 is shown in Figure 2 to be Kettle Bottom Shoals, and segment 12 to 14 is the deep trench around Morgantown.

A first impression is that the rectangular array of computational cells does not represent the bottom topography, and in particular, the bottom slope. The bottom topography and slope is, however, represented in detail by the widths. Connecting a given bottom width, say 400 m, which might represent the channel prism line, shows that the model has a realistic bottom variation and uniform bottom slope toward the river end regardless of the computational grid.

Boundary and Initial Conditions

The three time-varying inputs are tide at mouth, time-varying vertical salinity profiles at mouth, and freshwater inflow. Relative to model geometry, the tide and salinity are both specified in segment 22 which is outside of the Potomac. The geometry of segment 22 does not affect the computations at the mouth or upestuary. The first computed velocity profiles are at the right-hand boundary of segment 21 and represent the computed boundary velocities.

The tide height variation at the mouth is based on data provided in Rives (1973). The present simulations use a simple sinusoidal tide with a 0.20-metre amplitude and 12.45-hr period. The diurnal inequality is not considered in these simulations, nor are the longer term mean water level changes over a few days

by wind. The latter requires a measured tidal record at the mouth. The data input formats and time-varying data selector of LARM are capable of handling these records, but the records were not readily available for these simulations (Boicourt, 1980).

Time-varying vertical salinity profiles are required at the boundary. Hourly salinity periods of September 4 to 7, 1974, and September 9 to 14, 1974, for stations located at 10 and 19 nm (P10 and P19) from the mouth. These stations are at the down-estuary end of model segments 19 and 17 respectively (Figure 2). They are too far upestuary to provide boundary salinity data but can be used for comparisons to model results. Longitudinal-vertical salinity profiles extending to RM 02 nm are given in Elliott (1976) approximately once a month including August and September 1974. Examination of the salinity profiles from one time to another and the hourly data in Elliott and Hendrix (1976) shows only small hourly salinity changes at P10 over the period. For purposes of the test simulation, the RM 02 nm salinity profile given in Elliott (1976) is used at the boundary and assumed constant over time. The time-varying data selector developed for model applications is quite capable of handling time-varying vertical salinity profiles when that boundary data is available.

Initial conditions refer to the values of all computed variables specified at interior points from which the computation is started. The numerical time integration of the laterally averaged waterbody dynamics written in LARM and the time stepping procedure is such that one can begin with zero velocity components

and constant constituent concentration, or in the case of an estuary zero salinity, and let the computations interate to a time-varying solution from the boundary data alone. This was not done for the Potomac because it takes approximately 30 to 60 simulated days to achieve an internal distribution for salinity. However, it requires only two or three tidal cycles to establish periodic water surface profiles and velocity profiles. A solution to this problem is to specify the initial salinity distribution either from measurements or previous computations. The profile in Elliott (1976) for August 21, 1974, was used to give the initial longitudinal and vertical salinity profiles. These are given in Table 2. The transient build up of salinity from boundary data is examined more fully in Part V.

Freshwater inflow to the Potomac estuary is from the river at Great Falls and numerous tributaries along the 100 miles of estuary. Although the model derivation and code includes tributary inflows, they were not used in the test simulation. The daily mainstream flow of the Potomac River for the period of August and September 1974 was taken from Elliott (1976).

Choice of Time Step

Choice of the integration time step depends on stability limits of the numerical formulation and for tidal cases with short-term variations it determines the resolution of the boundary data. Too long a time step means that the time-varying boundary data may be poorly represented. The LARM model is

implicity longwave and the time step is not restricted by the surface gravity wave criterion. It is, however, restricted by the Torrence condition $\Delta t \leq \Delta x/U$.

It is difficult to set Δt for an estuary, as opposed to a reservoir, because U is changing rapidly with time and can become quite large within the tidal cycle. Measurements on the Potomac indicated $U \tilde{=} 40$ cm/s max, and with $\Delta x = 9266.25$ m (5 nm), this suggests a Δt limit of 386 minutes or five hours. This is much too long to resolve the boundary tidal period as would be one hour or even 15 minutes. Because of the efficiency of the computation and the need to have good tidal averages of various results, it was decided to use a ten-minute (600-second) time step in the computations.

The numerical formulation does have an internal wave limitation as $\Delta x/\Delta t > \sqrt{gH\Delta\rho/\rho}$ since the horizontal density gradient component of the horizontal pressure gradient is lagged by a time step in computing surface elevations and velocity components. The $\Delta\rho/\rho$ for the Potomac, from S=0 ppt to S=15 ppt is 0.011, and H_{max} 20 m requiring $\Delta x/\Delta t > 1.466$ and $\Delta t < 6317$ sec or 105 minutes. The internal wave criterion is more restrictive than the Torrence condition.

Some runs were made at a Δt which divided the tidal period of 12.45 hours into an even number of increments. For example, a $\Delta t = 448.2$ seconds gives exactly 100 iterations per tidal cycle and allows the tidal boundary data to be resolved at approximately five-minute intervals.

Validation

Validation of the computational code determines if it gives correct answers for known situations. It is a step which checks the numerical computations by using relatively simple combinations of boundary conditions. Validation cases are set up to test for instabilities, computational errors, and errors in accumulation or loss of volume and salt. These would be errors related to formulation and coding. The estuarine boundary condition of LARM was run for the cases of constant river inflow at constant downestuary elevation, constant salinity at the downestuary boundary with no freshwater inflow, and a sinusoidal downestuary elevation.

The case of constant river inflow and constant downestuary elevation results in an upestuary surface slope and a computed outflow at the mouth. The crucial tests are that the outflow should eventually become equal to the inflow over time, and there should be no volume loss of water over time once the surface slope is established. These tests were all satisfied.

The case of constant salinity at the downestuary boundary tests the ability of the computed boundary condition to convect salinity into the estuary through the horizontal density gradient. It also tests representation of the salt front as it moves upestuary due to buoyant convection. The model showed the influx of boundary salts initially over the total water column. As time progressed, the influx of boundary salts was from the deeper portions of the water column and an outflow became established in the top portion of column as would be expected.

The sinusoidal elevation at the downestuary boundary represents the tidal forcing function. In certain spatial differencing forms of the basic momentum and continuity equations it can lead to producing higher frequency and shorter wavelength oscillations. It can also lead to alternating solutions on successive time steps. None of these problems were encountered using the estuarine boundary condition in the LARM code. The tidal wave computed by the model propagated up the estuary at the surface gravity wave speed. The computed flows in and out of the mouth of the estuary became periodic within a few tidal cycles and did not show any differences from one tidal cycle to the next.

Simulation Results

The first results of interest from the simulations are the spatial and temporal variation of tide height and the pattern of circulation throughout a tidal cycle. The simulation was run for ten days to remove effects of initialization and detailed hourly results were examined for the last tidal cycle. It was determined that initialization effects were overcome and stationary conditions reached by comparing velocity components at a given location from one tidal cycle to the next.

The velocities were started from zero and essentially established a repetitive pattern within two tidal cycles. After that small adjustments of tenths of cm/sec took place in response to time-varying freshwater inflow and gravitational circulation related to changes in salinity.

Salinity was initialized at the values in Table 2. The salinity distributions at the end of ten days are shown in Table 3. Compared to the initial salinity distributions, the salinity after ten days shows a very large adjustment from model segment 10 at river mile 58 upestuary to the head of tide. This computed change in salinity does not appear to follow the smaller salinity changes found in Elliott (1976) between August and September 1974, for the upestuary stations.

The modes of circulation over a tidal cycle--can be examined simultaneously as the water surface elevation and velocity vectors. These are shown for every two hours through the tidal cycle in Figures 3 to 9. The velocity vectors are exaggerated in the vertical by the horizontal to vertical scale of the depth profile. An example of the exaggeration is found near 110 km. The vectors show a vertical displacement of about 2 metres over four hours at the same time that upestuary horizontal motion is about 5 km.

The water surface elevation for the first hour of the tidal cycle shows a high tide at the mouth of the estuary simultaneously with a low tide at the head of the estuary. It is a wave with a node point near RM 50 which is at a sharp bend in the river. The circulation follows the water surface elevation changes while it is also responding to the horizontal density gradient. In Figures 3 to 9 as the circulation is followed from hour to hour, it is seen that the upper end of the estuary continues to flood while the lower portion is ebbing as the circulation responds to the surface wave (day 10.1181).

Figure 3. Water Surface Elevation and Circulation Pattern at 0.8 Hours after High Tide at the Estuary Mouth

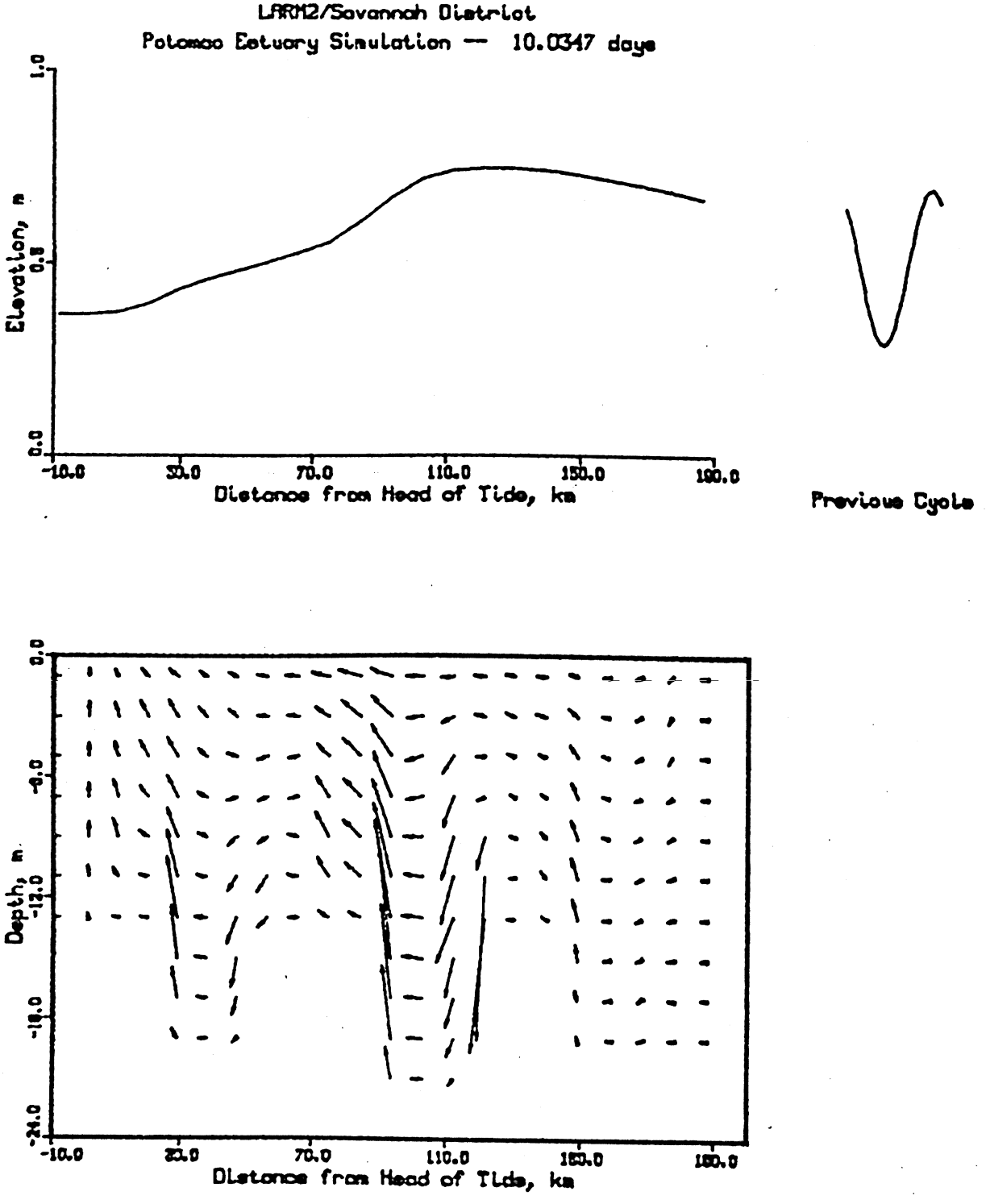

Figure 4. Water Surface Elevation and Circulation Pattern at 2.8 Hours after High Tide at the Estuary Mouth

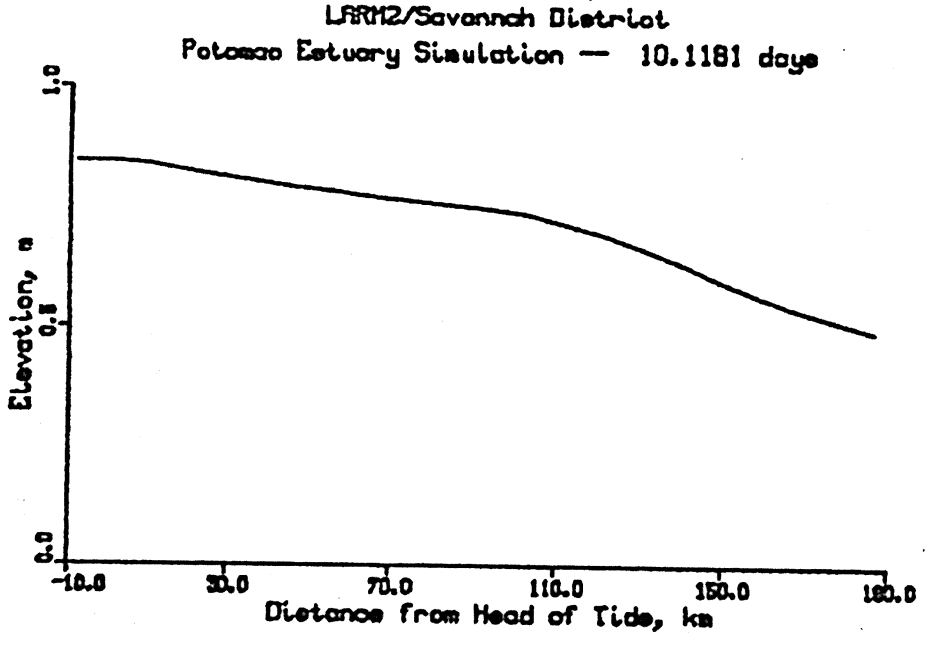

Previous Cycle

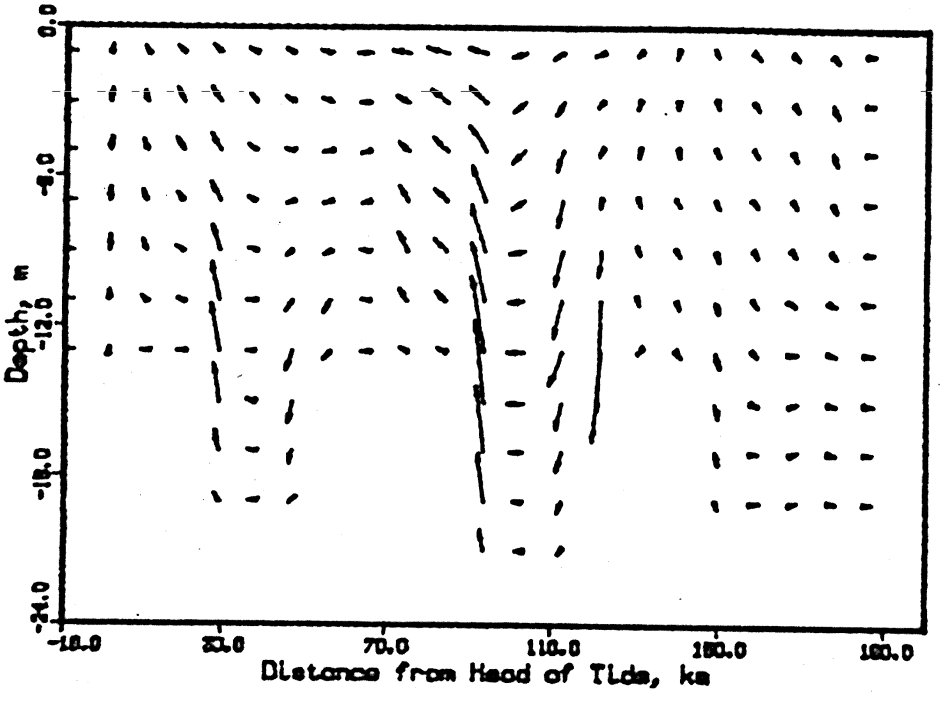

Figure 5. Water Surface Elevation and Circulation Pattern at 4.8 Hours after High Tide at the Estuary Mouth

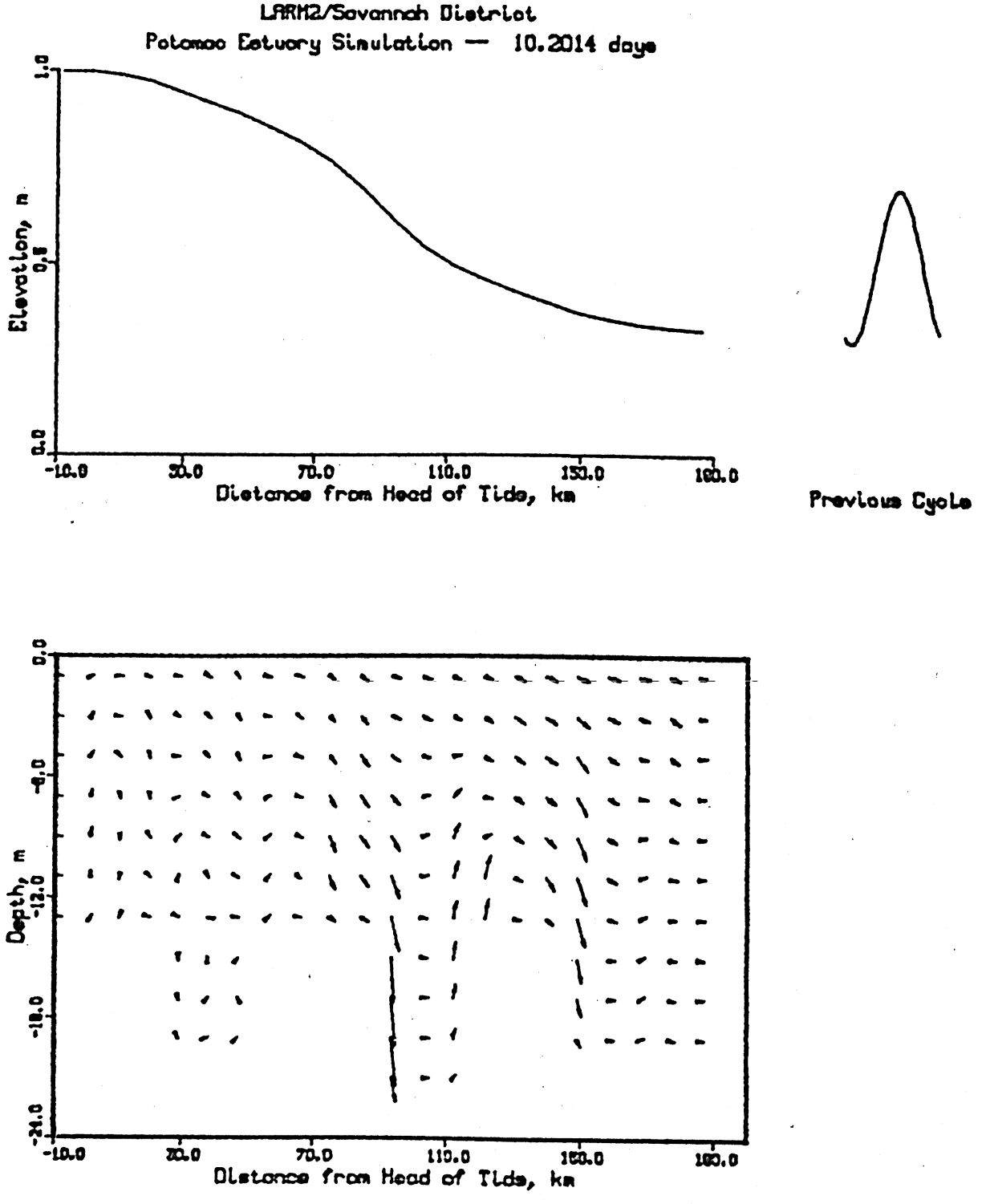

Figure 6. Water Surface Elevation and Circulation Pattern at 6.8 Hours after High Tide at the Estuary Mouth

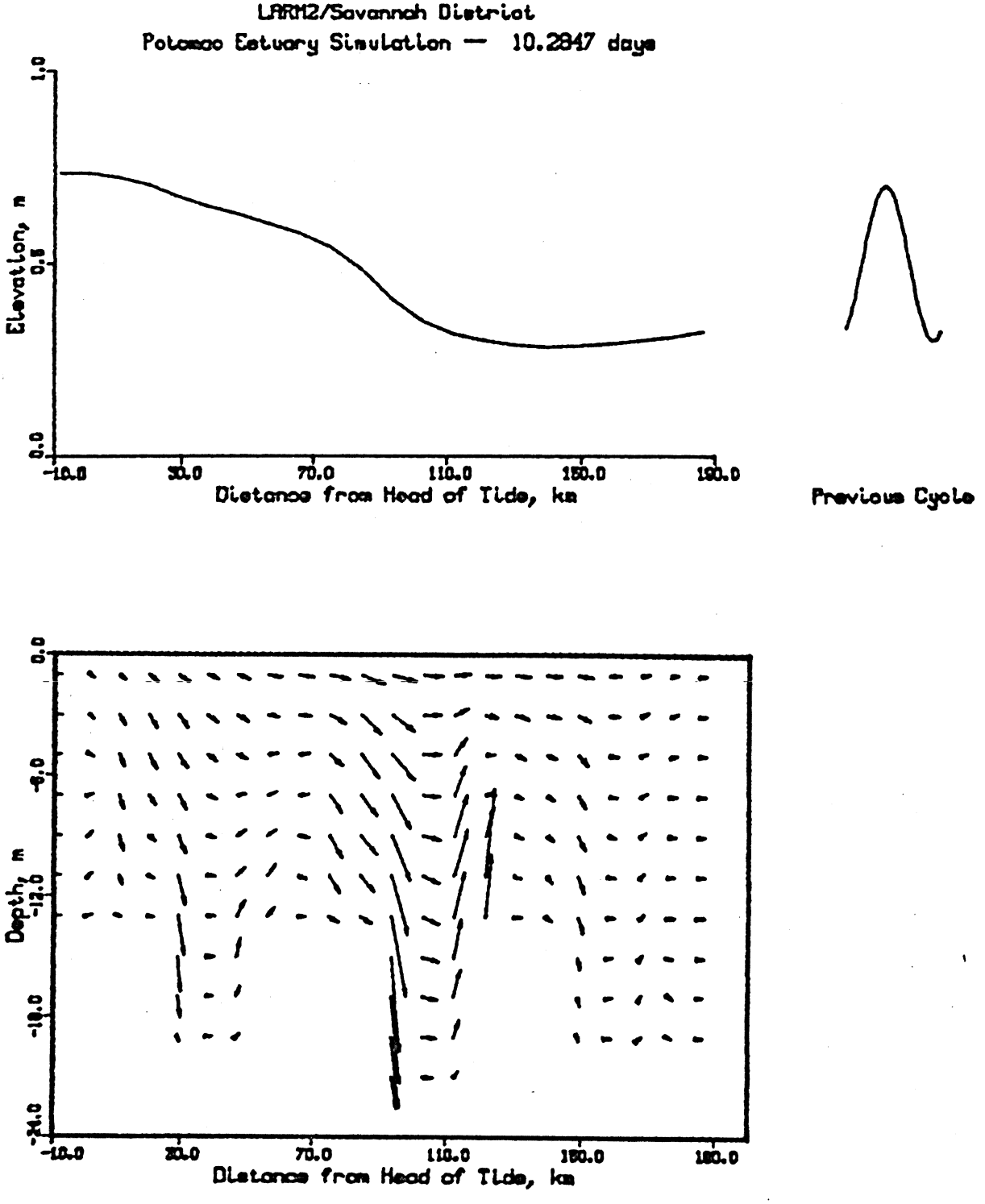

Figure 7. Water Surface Elevation and Circulation Pattern at 8.8 Hours after High Tide at the Estuary Mouth

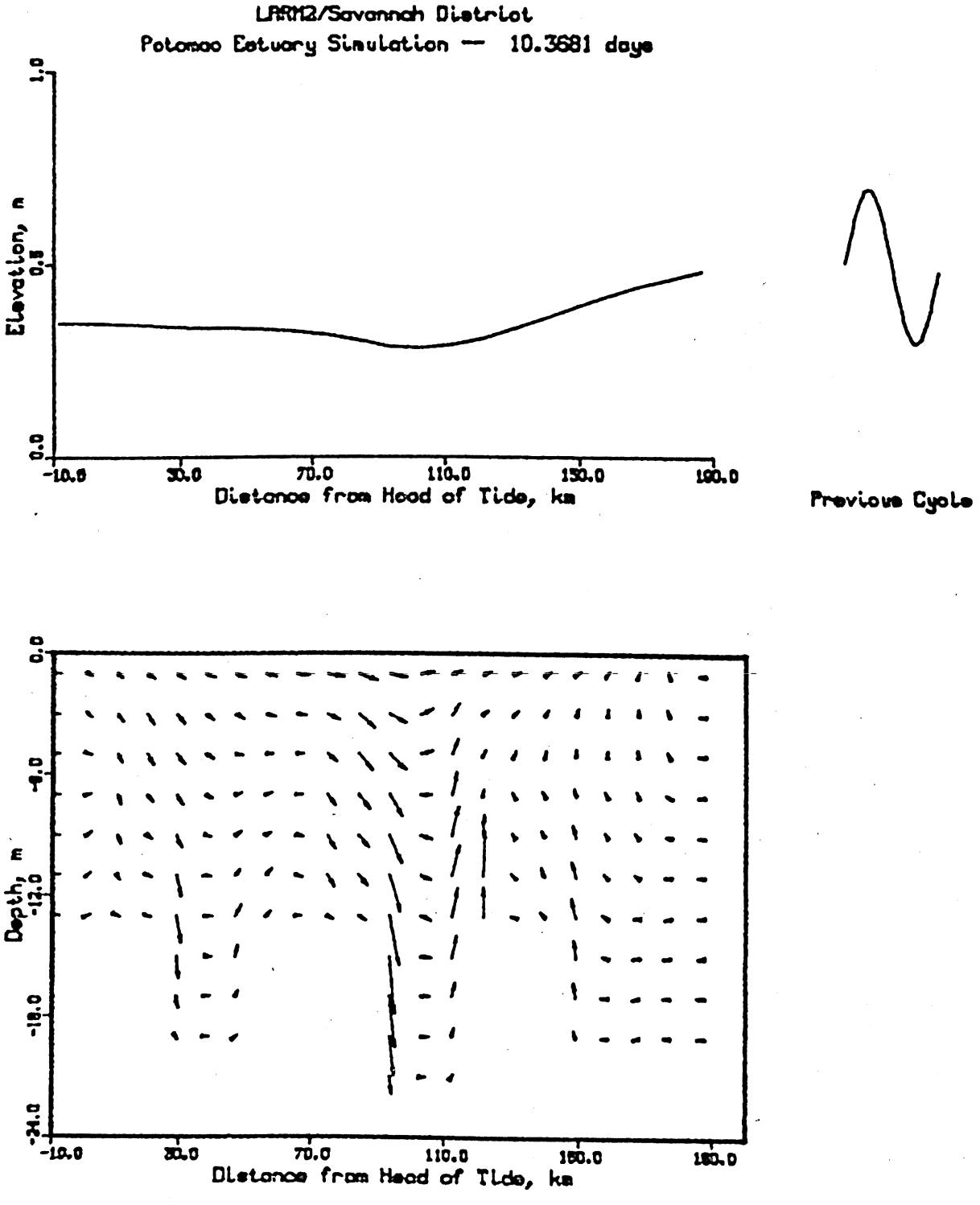

Figure 8. Water Surface Elevation and Circulation Pattern at 10.8 Hours after High Tide at the Estuary Mouth

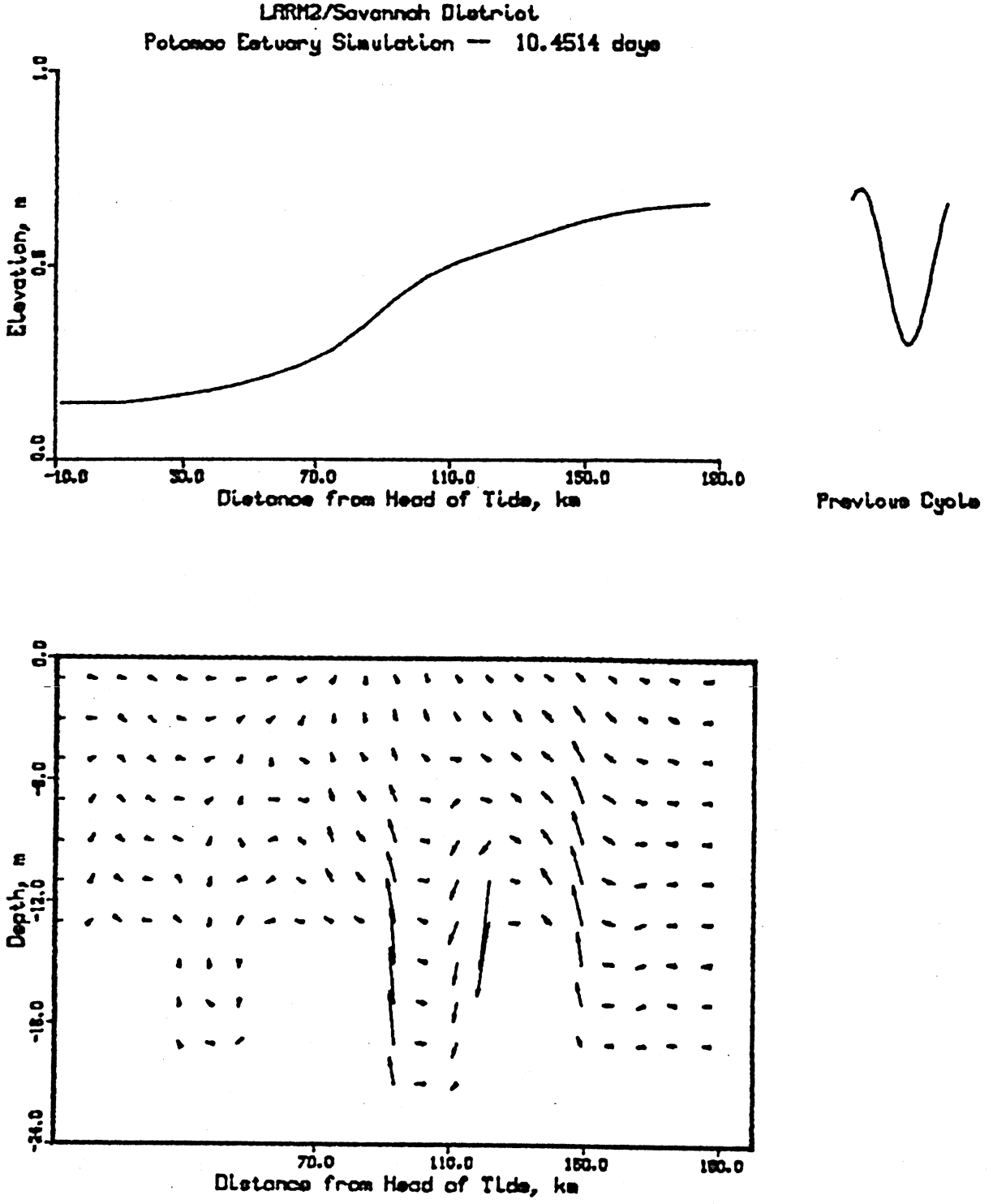

Figure 9. Water Surface Elevation and Circulation Pattern at 12.8 Hours after High Tide at the Estuary Mouth

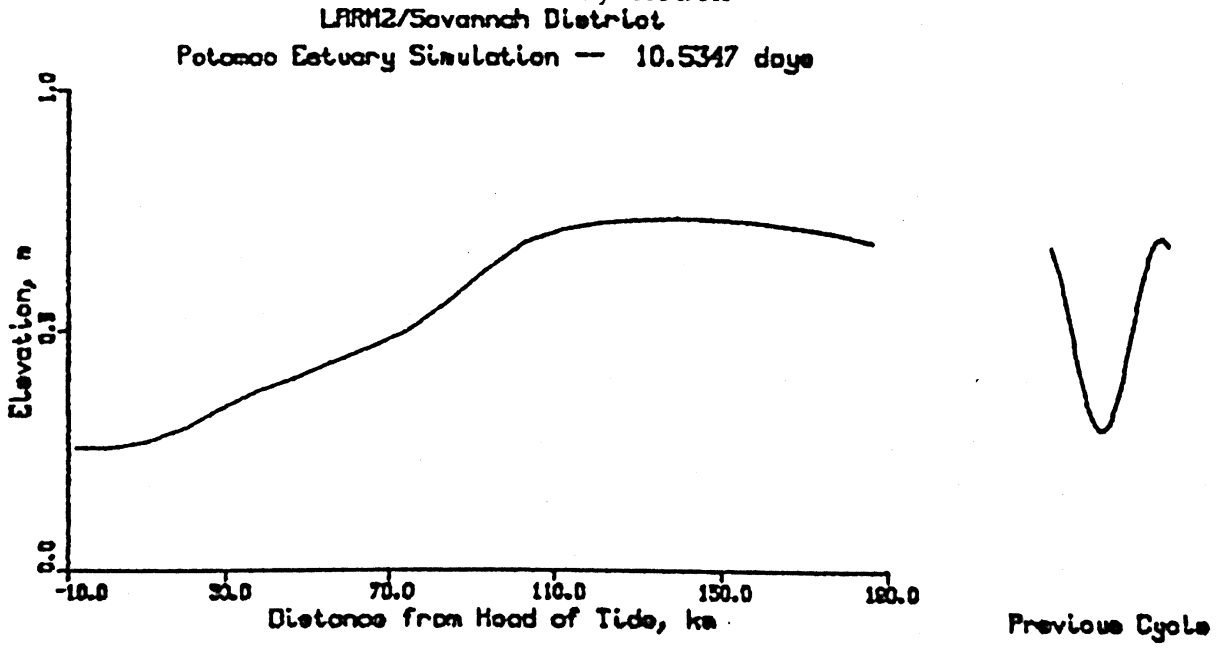

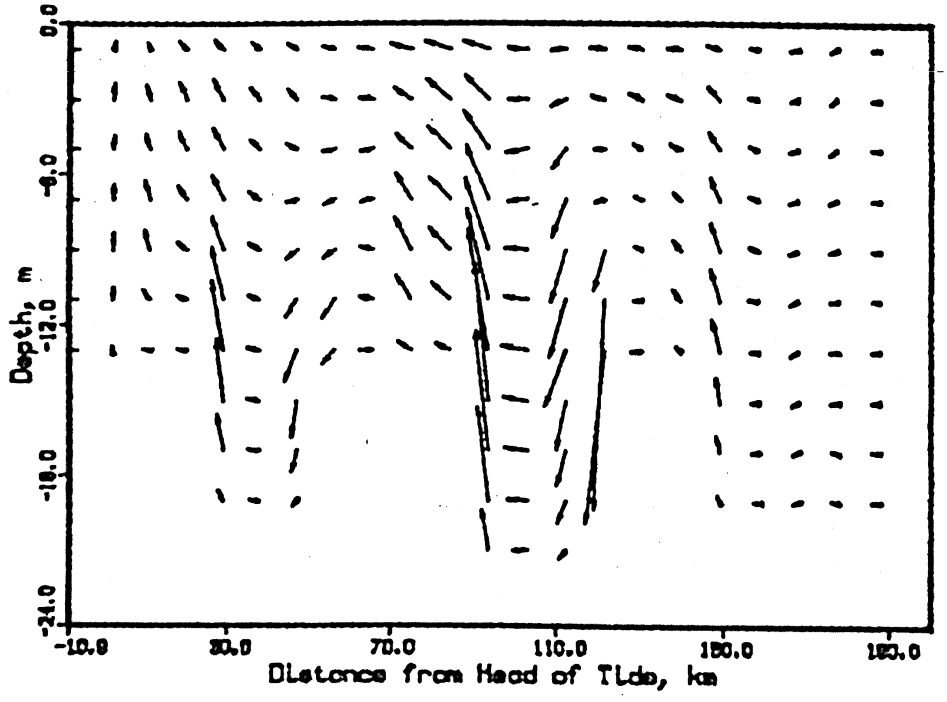

There is some indication of two-layered flow toward the end of the tidal cycle (day time 10.3681) which shows that the flooding tide at the estuary mouth is mostly in the bottom layers.

There is a tendency for the magnitudes of the velocity vectors at a given time in the tidal cycle to follow the geometry of the estuary. The strongest flows are at the constricted cross section near model segment 11 which is also one of the more shallow portions of the estuary. Velocities are smaller throughout the tidal cycle in the lower portion of the estuary because of its greater cross-sectional geometry (Table 1).

Overall flushing and transport through the estuary is eventually related to the tidally averaged circulation. The computed tidally averaged circulation for the Potomac is shown in Figure 10. Here the vector lengths represent displacement over 24 hours. It is a result of averaging the velocity vectors at each point over a tidal cycle at ten-minute intervals.

The computed boundary velocities are at the mouth of the estuary near 190 km. From Figure 2, this is at the boundary where the Potomac enters Chesapeake Bay. The boundary velocities are computed from the specified tide height in the bay and the simultaneously computed tide height for the first model segment in from the bay (segment 21). The velocities at the mouth show a tidally averaged profile of intrusion in the bottom layers and an outflow in the surface layers. This pattern follows upestuary where at each cross section there is a distinct depth at which the vectors change from having an

Figure 10. Potomac Estuary Tidally Averaged Circulation for Period given in Figures 3 to 9

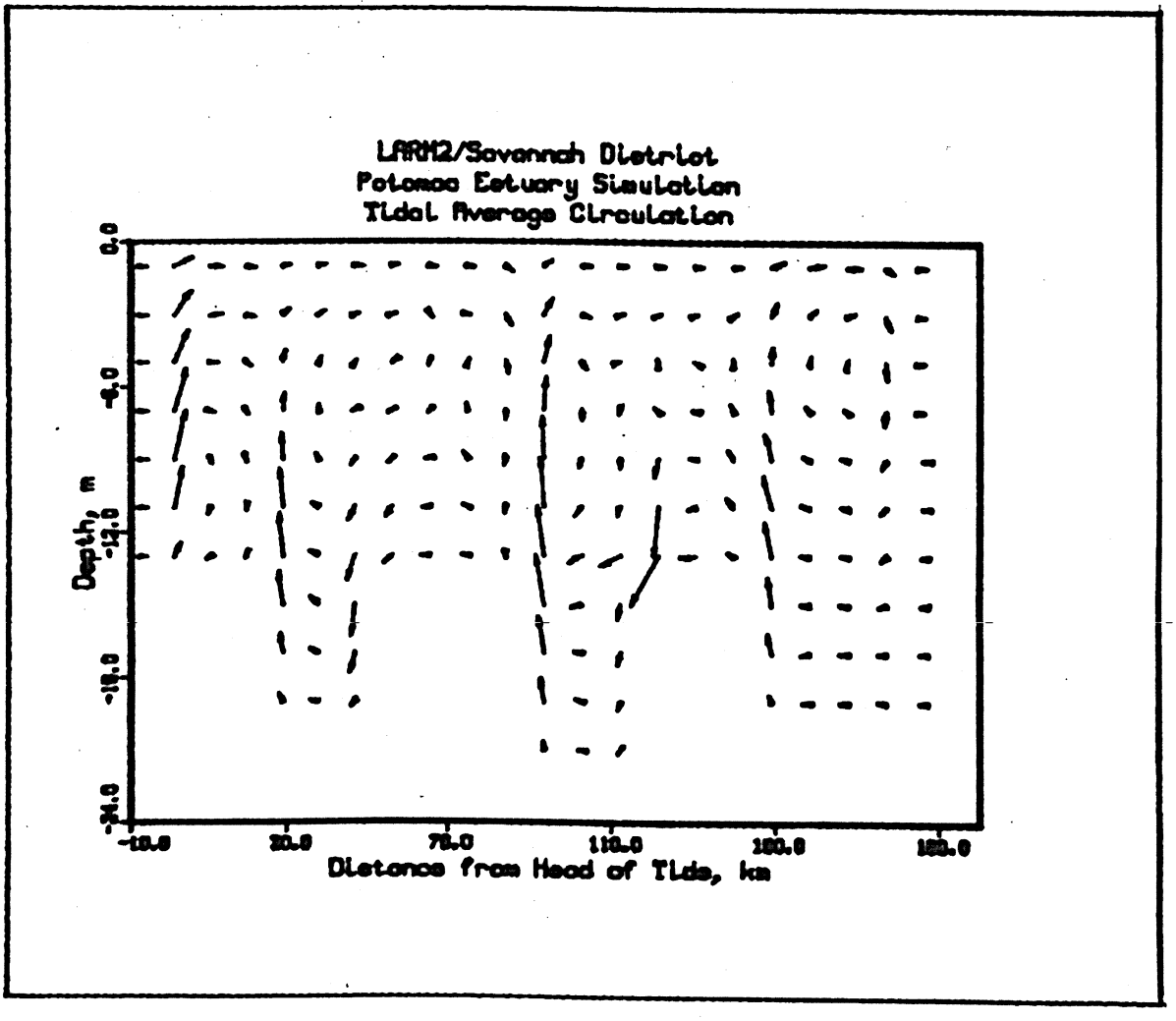

upestuary component to a downestuary component. Overall, the estuary tends to circulate in two parts: an upestuary part above 80 km at the narrows and a downestuary part. There is a net flow between the two parts represented by the bottom water intrusion near 80 km.

The tidally averaged circulation shown in Figure 10 tends to have a circular pattern near the estuarine mouth. There is a slight downflow from the surface layer to the bottom layers in the last segment before the boundary outflows. Since the computation of the outflow boundary velocities does not include the horizontal advection or dispersion of momentum, the circulation may result from dissipation of momentum from the interior flow at the boundary. The magnitude of the rotary circulation is not as large as indicated in Figure 10 because of the exaggerated vertical velocity.

PART IV: PREDICTED AND OBSERVED TIDAL DYNAMICS

The availability of survey data on the Potomac River estuary allows quantitative comparisons of predicted model results and observed tide height and velocity conditions. Tide height information is available in some form along most estuaries. It may be time and height of low and high water forecasts as a minimum or detailed tide height measurements over a specific period of time. The difference is that the latter includes wind and freshwater runoff effects while the former includes only solilunar effects. Wind and freshwater runoff influences the mean water level over a number of days, and their effect on the downestuary boundary are important for proper computation of boundary inflows and outflows.

Detailed velocity profiles are not routinely obtained for estuaries. Special studies of the Potomac were conducted by the Chesapeake Bay Institute and reported in Elliott and Hendrix (1976) for two periods, September 4 to September 7, 1974, and September 9 to September 14, 1974, at two stations. One station was 10 nm from the mouth and the other was 19 nm from the mouth. Velocities were measured at 1-metre intervals hourly. These velocity profiles are used for detailed comparison to the model results.

Vertical dispersion coefficients and vertical velocity components were not computed for the Potomac data. They are, however, an important part of the model since they are a major transport mechanism. The model results are compared

qualitatively with the properties of vertical dispersion coefficients and vertical velocity components inferred by Pritchard (1967) from the James River studies. The James River studies are also summarized in Officer (1976).

Tide Heights

The predicted model tide heights over time for various stations along the Potomac are given in Figure 11. The tide is driven at the mouth (186.25 km) with an amplitude of 0.2 m. Upestuary at 28.73 km, the tide range tends to increase and there is a phase shift of high tide to occur later than at the mouth. The range and phase shift of the observed tides have been summarized for the Potomac by Rives (1973), and can be used for comparison to the computations.

Tidal ranges are compared in Figure 12. The model results are given for various values of bottom friction since this is the major variable that influences tidal amplitude in the model. The observed tide range shows a local maximum upestuary from the mouth, a minimum near model segment 11 (Figure 2), and increase to the head of tide. The observed tide range minimum coincides with the nodal point of the standing tide wave.

The computed results show that the model runs satisfactorily over a wide range of friction factors with no numerical difficulties Numerical schemes that lag many terms often fail at low friction (high Chezy C) since this term often maintains numerical stability. The change in tide range from the mouth to the head of tide is reproduced by the model for a C=60 $m^{\frac{1}{2}}/s$. The minimum at 90 km is reproduced for a C=40 $m^{\frac{1}{2}}/s$.

Figure 11. Time-varying Tide at Selected Stations along the Potomac River Estuary Computed for a Sinusoidal Tide at the Mouth

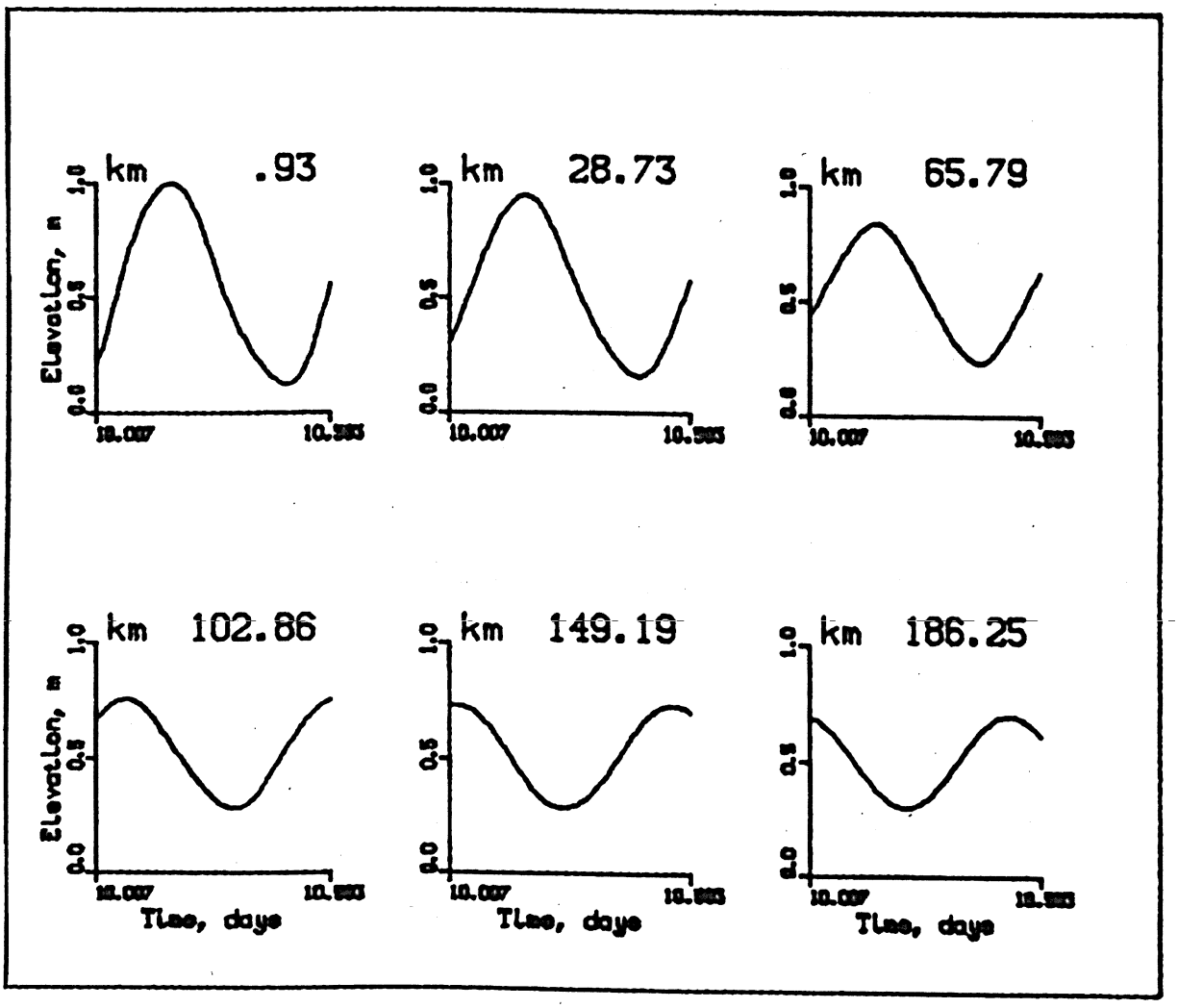

Figure 12. Comparison of Observed and Predicted Tidal Ranges along the Potomac Estuary

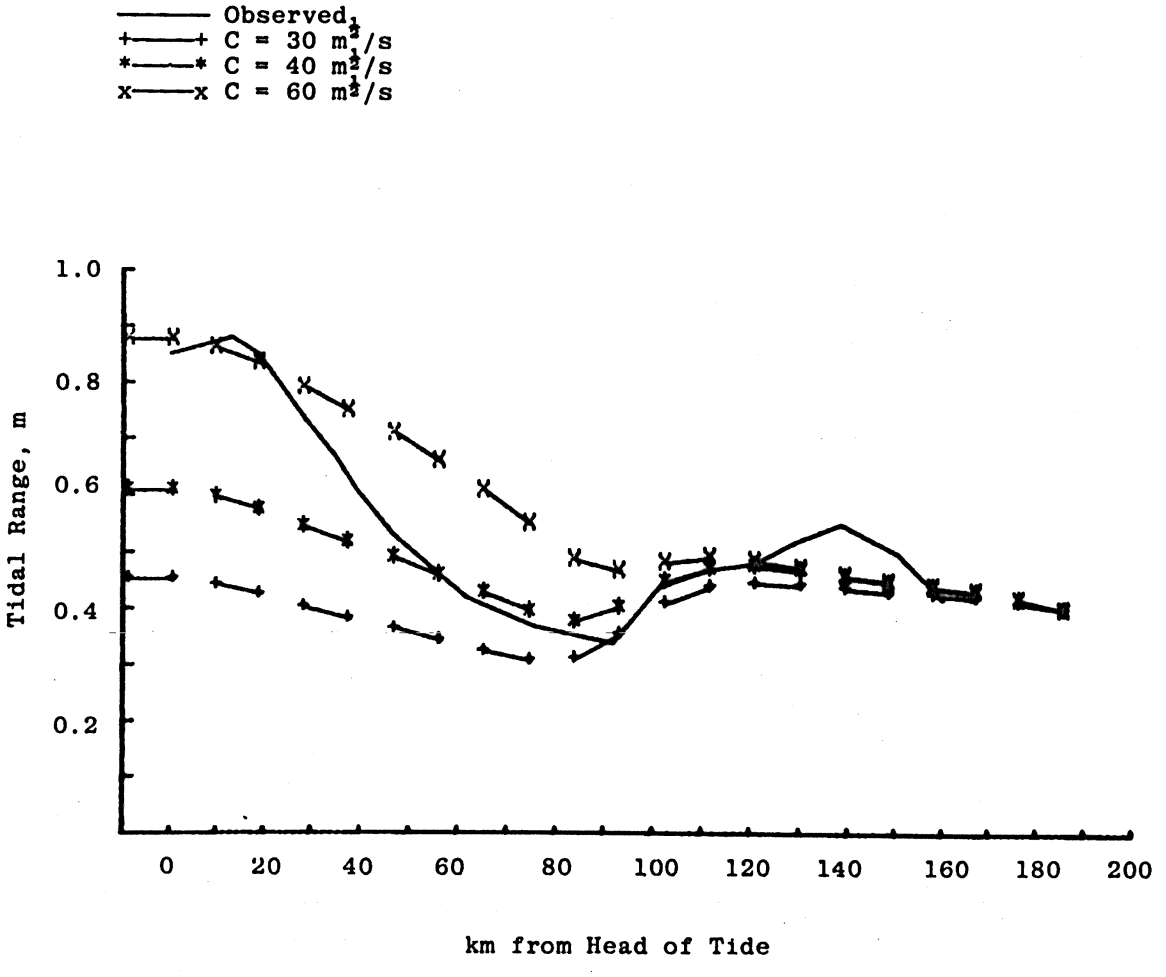

The model could be tuned to tide range and phase by varying the friction coefficient longitudinally along the model. Rives (1973), however, shows with a one-dimensional tidal model with detailed spatial averaging that the Potomac estuary tidal range minimum is reproduced for a spatially uniform friction coefficient. Varying the friction coefficient spatially in a coarse spaced grid as used in the present simulation thus appears partially to be a surrogate for spatial detail. There are, however, changes in cross-sectional geometry for which changes in the friction coefficient is justified.

The phase lag of the tide height from the mouth of the estuary can be compared for observed and computed conditions. It is given for various friction coefficients in Figure 13. There is a tendency for the model to underestimate the phase lag at the head of the estuary. There is little variation in the computed phase lag with friction coefficient since phase lag mostly depends on gravity wave propagation. Propagation of the tide wave up the estaury is primarily governed by the gravity wave speed ($\sqrt{gH}$) which is solely function of depth. The computed wave would be based on the geometry given in Table 1 and this may vary from the real geometry related to wave propagation. The difference in observed and computed tide phase, based on the results of Rives (1973), may be due to the geometry resolution in the model.

Velocity Distributions

The real test of the model is the degree to which it reproduces observed temporal variations in velocity. A valid

Figure 13. Comparison of Observed and Predicted Tidal Phase along the Potomac Estuary

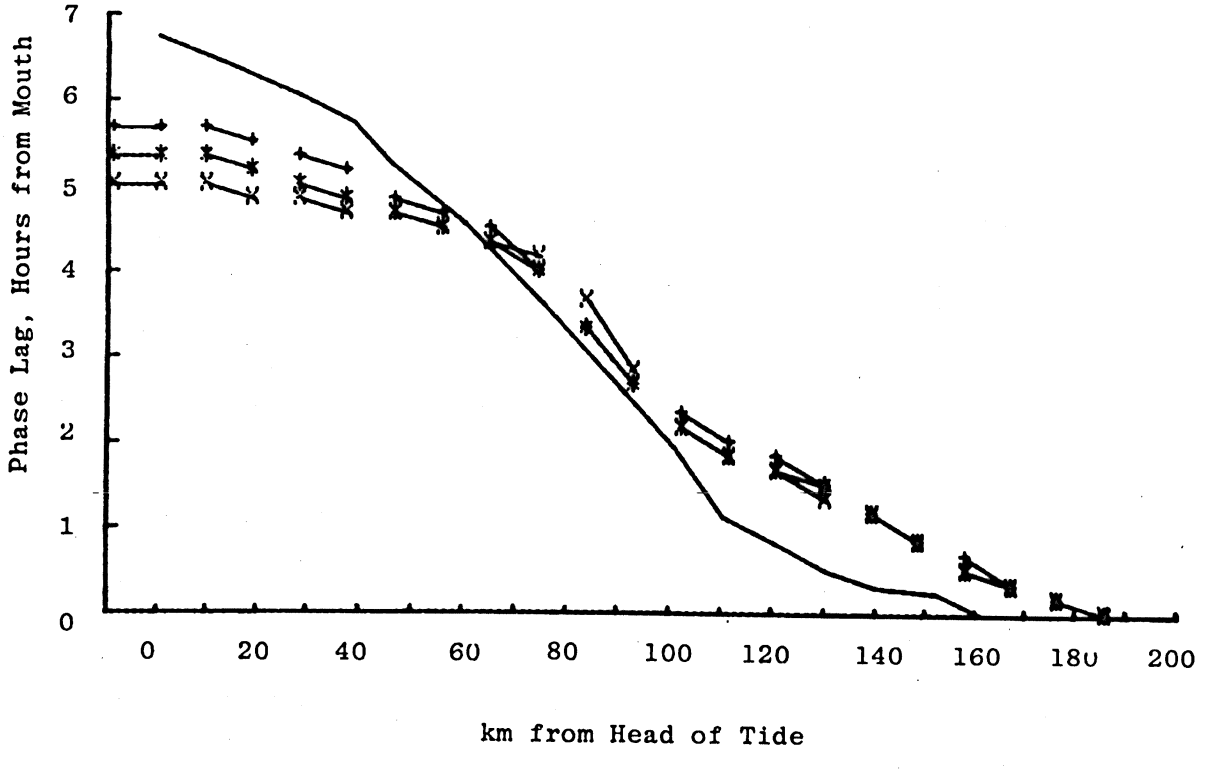

comparison depends on how well the boundary conditions during the period of observation are represented in the model. Conditions during the Chesapeake Bay Institute (CBI) September 1974 surveys are given in Figure 14 including the residual or long-term change in tide height at the estuary mouth, and the wind shear stress along and across the estuary.

The detailed tide and wind record for the period of observations used in Figure 15 are no longer readily available (Boicourt, 1980). Lacking the actual data, the model is run for the simpler condition of a sinusoidal tide with no mean elevation change and no wind. The latter conditions appear to be satisfied for the first 18 hours of the September 9 to 14, 1974, survey period shown in Figure 14. The hourly velocity and salinity profiles at station P19 are used for showing the comparison to the model results. The results at station P10 were similar to P19. Deviations from the model conditions are examined as part of a sensitivity analysis.

The computed and observed velocities at 2-metre depths are compared for survey station P19 in Figure 15. Since a sinusoidal tidal height at the mouth is used in the model, the relationship between the tide phase and the day-hour is not known precisely. The computed velocities at one depth were shifted in phase until they coincided with the observed velocities. The sinusoidal tidal boundary in the model does not include any diurnal inequality which might have been in the real tidal record. The computed velocities reproduce the maximum and minimum velocities at all

Figure 14. Tide and Wind Conditions during Study Period. E_2 (cm), the Residual Elevation at Colonial Beach; W_1 ($m \cdot S^{-1}$) Downestuary Wind; W_2 ($m \cdot S^{-1}$) Cross-Estuary Wind, from NE to SW. (from Elliott and Hendrix, 1976)

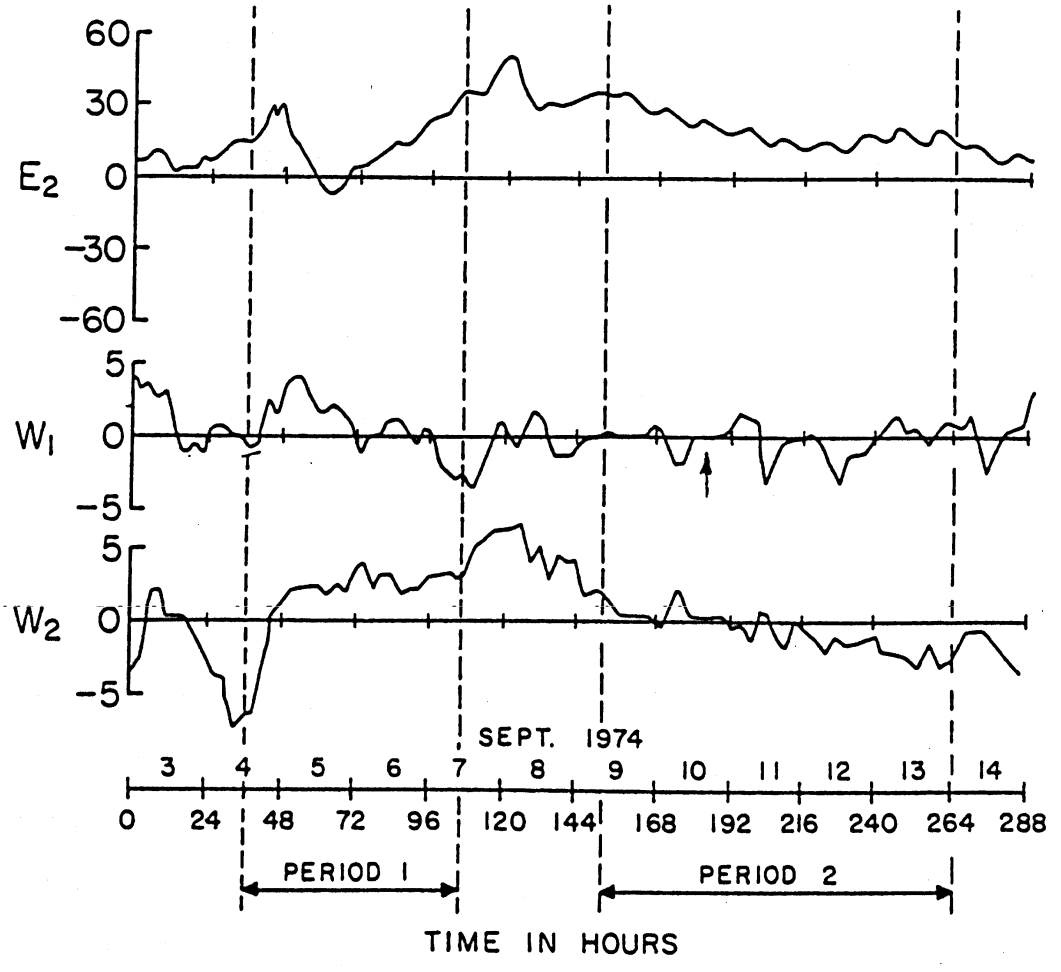

Figure 15. Comparison of Observed and Computed Velocities at Station P19 for the Indicated Depths

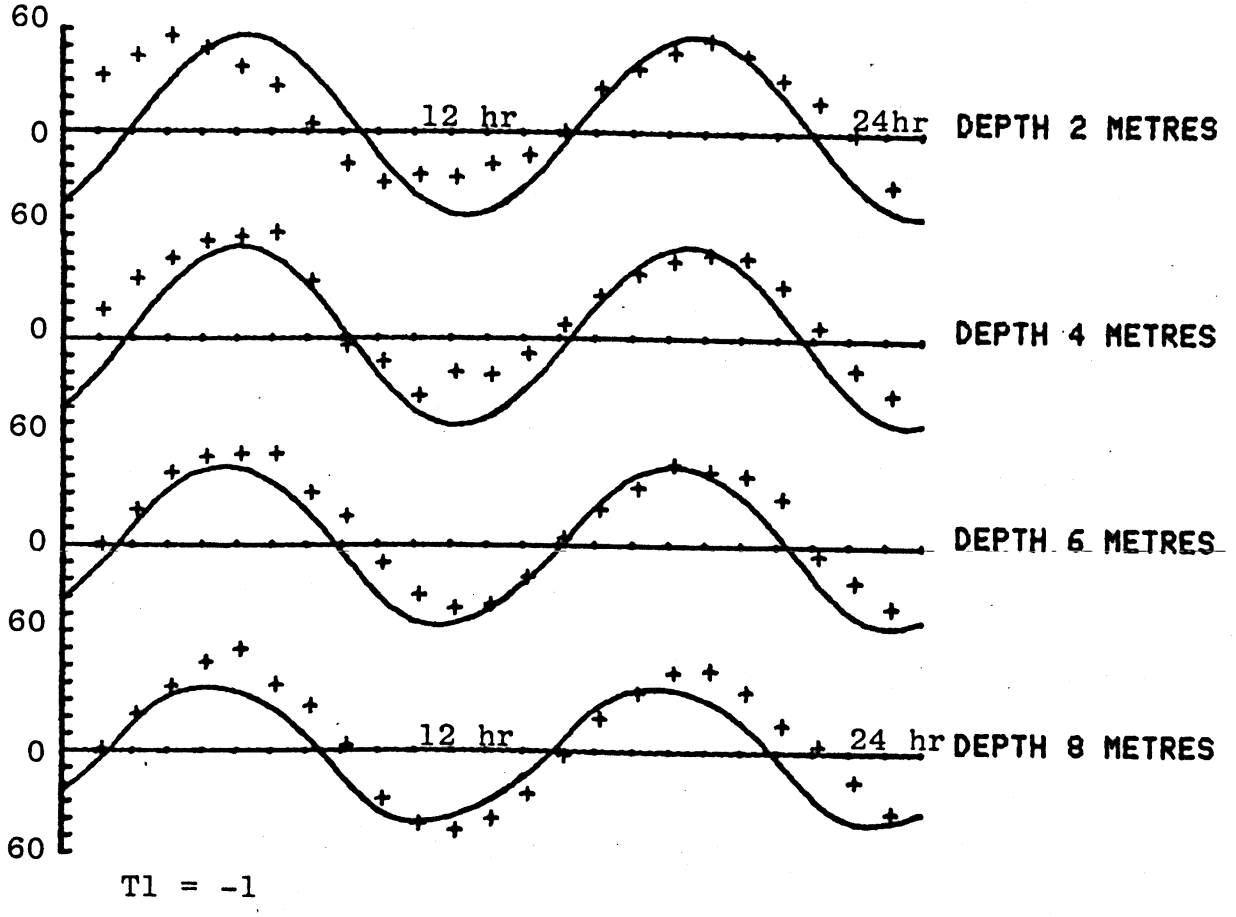

depths and except for the surface velocities, the model reproduces the shape of the observations. The surface velocities are distorted by wind.

Important characteristics of estuarine tidal velocities are shown in the data and reproduced by the model. In a stratified estuary exhibiting a two-layered circulation like the Potomac, the tendency of the velocity is to have a stronger ebb than flood velocity in the surface layers and to have a stronger flood than ebb velocity in the bottom layers. This characteristic is shown in the data presented in Figure 15 and is reproduced by the model.

Detailed comparisons of the vertical velocity profiles are given in Figure 16. Model profiles were available every 20 minutes and observed profiles available every hour. The phase shift of the computed profiles of Figure 16 was nine minutes, thus the observed and computed profiles do not coincide exactly. The model profiles produce the magnitude of the observed velocities throughout the tidal cycle and reproduce important profile features. Beginning toward mid-tide at 0800 hours, the bottom velocities begin to flood while the surface velocities are still ebbing. This continues until the full flood tide velocity profile is developed and then the bottom velocities begin to ebb before the surface velocities.

The tidally averaged velocities are a fraction of the ebb and flood maximum velocity, but the net circulation and flushing of the estuary is determined by the tidally averaged velocity.

Figure 16. Computed and Observed Velocity Profiles at Station P19 Potomac Estuary for September 9-10, 1974, Taken Hourly through One Tidal Cycle

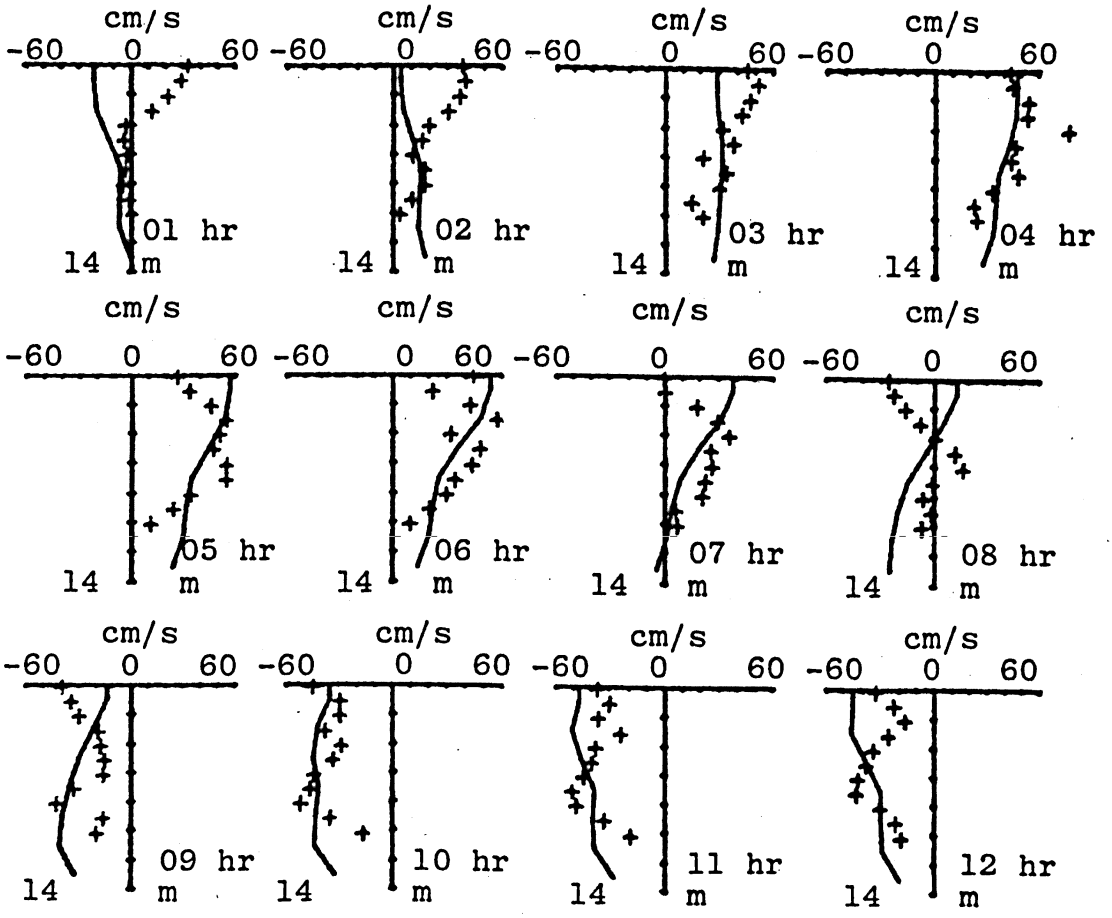

The tidally averaged and ebb and flood maximum velocities are shown in Figure 17 along with the tidally averaged salinity profile. The tidally averaged velocity profile is the classical case of a surface layer outflow and a bottom layer inflow. The model reproduces the depth of the velocity interface and the bottom layer velocities. The surface layer velocities deviate from each other because of wind effects.

The observed and computed maximum ebb and flood velocities agree except in the lower portion of the water column. The observations show a flood tide maximum with depth in the bottom layer that has also been observed by Pritchard (1967) which is not reproduced by the model.

Salinity Distributions

The tidally averaged salinity profile is shown in Tables 2 and 3. The salinity profile changes very little throughout the tidal cycle at stations close to the estuary mouth unless there are changes in the boundary salinity. The computed salinities would be expected to match the observed salinities because observed salinities at an earlier date were used to initialize the model computations. Unfortunately, there are no detailed salinity profiles further upestuary during the CBI surveys.

It is expected that salinities in the upper reaches of the estuary are more variable than in the lower estuary. In the upper estuary, the salinity is an order of magnitude lower and a small variation is a greater percent change. In the upper estuary, salinity is controlled more by freshwater input than

Figure 17. Computed and Observed Tidal Averaged Velocity Profile and Maximum Ebb and Flood Velocities at Station P19 Potomac Estuary for September 9-10, 1974 Survey Period

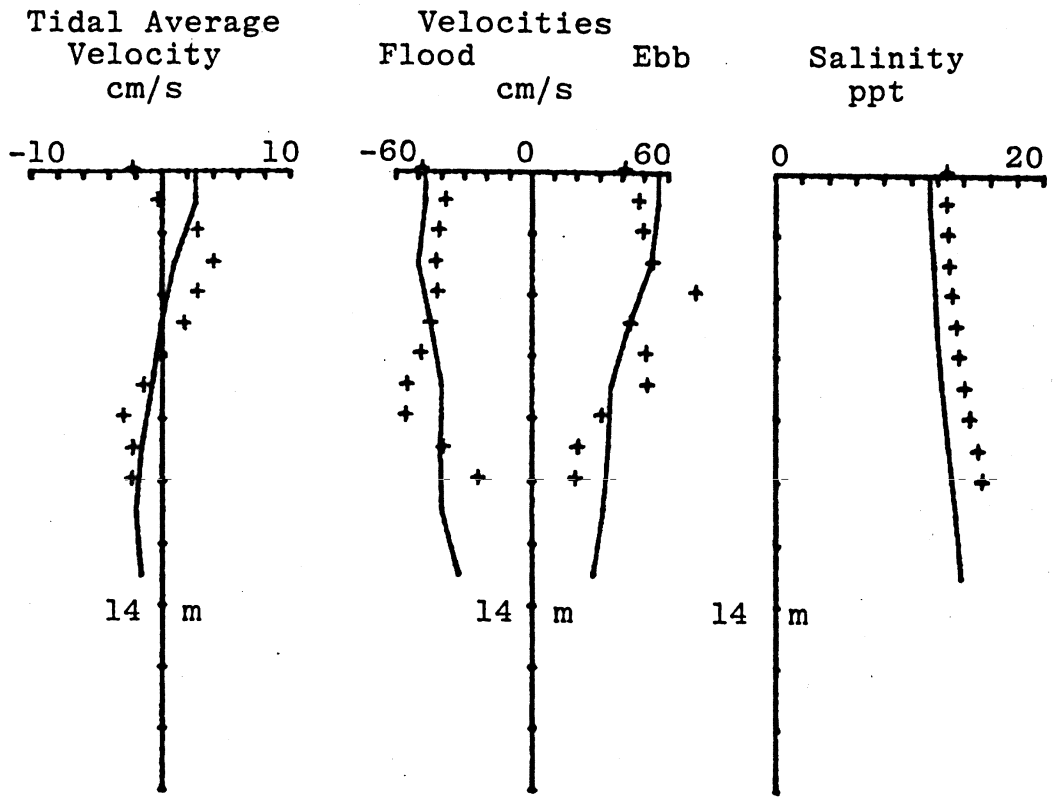

tide and salinity at the mouth. Except for comparing changes in salinity profiles over a long period of time as in Tables 2 and 3 from initial conditions to stationary conditions, there was no detailed profile station of salinity and current in the upper estuary for more detailed comparison of salinity variations.

Vertical Velocity Components

The computed ebb, flood, and tidally averaged vertical velocity component at RM 10 is given in Figure 18. The tidal average is an order of magnitude smaller than the maximum ebb or flood values, and its consistency in comparison to observations is a measure of its accuracy. The tidally averaged vertical velocity component is about 1/200 of the horizontal velocity component. The vertical transport of mass and constituent related to this low velocity is, however, large in the finite difference model because of the larger area through which it is transporting. In a model segment, the ratio of bottom area to end area is as $\Delta x/H$ and for the Potomac simulation this ratio is 2500, thus the vertical transport can be as large as the horizontal transport.

The vertical velocity component cannot be measured directly. Pritchard (1967) has, however, computed a vertical velocity component profile in the James River using up- and downestuary velocity transects and salinity profiles over time and evaluating numerically various terms in the momentum and salt balance. These calculations showed that for a partially mixed estuary the tidally averaged vertical velocity component should be upward

Figure 18. Computed Vertical Velocity Component Profiles as a Tidal Average and Maximum and Minimum for Station P10

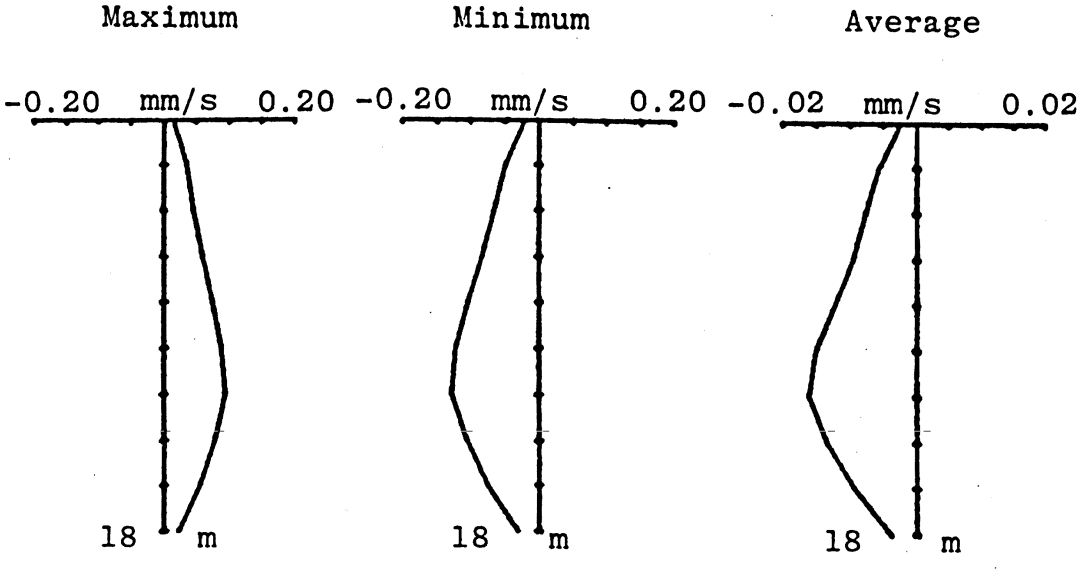

from the bottom to the surface layers, should be zero at the bottom, and the surface should have a maximum in the bottom layers. Figure 18 shows that the vertical velocity component profile produced by the model has the expected properties. The magnitude of the vertical velocity component is similar to that found by Pritchard (1967).

Vertical Dispersion Coefficients

The theoretical aspects of the vertical dispersion relationship in numerical models for estuaries and other waterbodies was discussed in Part II. The Munk and Anderson (1948) Richardson number dependency of the vertical dispersion coefficient on stratification is used for the present simulations. In order to examine the dependence of vertical dispersion on the Richardson number alone, A_{z_0} in Equation 22 was taken as a constant of 6×10^{-4} m^2/s for both momentum and salt.

Increasing the Richardson number in Equation 24 either by increasing stratification or decreasing velocity shear, decreases A_z. A lower value is set for A_z as the molecular value of momentum and salt diffusion. Decreasing Ri increases A_z toward an upper limit. When Ri is <0.10 or $\partial\rho/\partial z$ is negative due to vertical density instability, A_z is allowed to approach a maximum value of $H^2/(2\Delta t)$ where H is the layer thickness for the finite difference computation. This upper limit assures that there is no numerical instability due to the time lagged vertical gradient terms.

The Richardson number enters the dynamic computations as a local value. It is computed at each layer for each time step and is used to compute a local A_z. The vertical dispersion coefficient is thus being computed continuously with the local velocity and density gradient on which it depends. The variation of the vertical dispersion coefficient over depth and throughout a tidal cycle is given in Figure 19. It is computed using the velocity profiles shown for the same times in Figure 16 and for the salinity profile given in Figure 17. The salinity profile at staion P19 does not change substantially with time. Most of the change in the A_z profile throughout the tidal cycle is due to changes in the vertical velocity gradient over time.

Pritchard (1967) gives an estimate of the vertical distribution of vertical dispersion as derived from the James River data. It shows A_z being minimum or near zero at the surface and bottom, and a minimum at mid-depth near the region of maximum salinity stratification. The A_z computed from data by Pritchard (1967) had maxima in the mixed surface layers and bottom layers. The A_z computed by the model shown in Figure 19 exhibits all of the observed properties throughout the tidal cycle. The maximum value of 6×10^{-4} m^2/s is similar to that computed from data by Pritchard (1967). During most of the tidal cycle the model A_z shows upper and lower layer maxima as found from data.

The A_z distribution at hour 7 and 8 into the tidal cycle shows little or no mid-depth minimum. The velocity profiles in Figure 16 show that at hour 7 and 8 the bottom layer velocity

Figure 19. Computed Vertical Dispersion Coefficients for Station P19 Hourly through a Tide Cycle Corresponding to Velocity Profiles in Figure 16

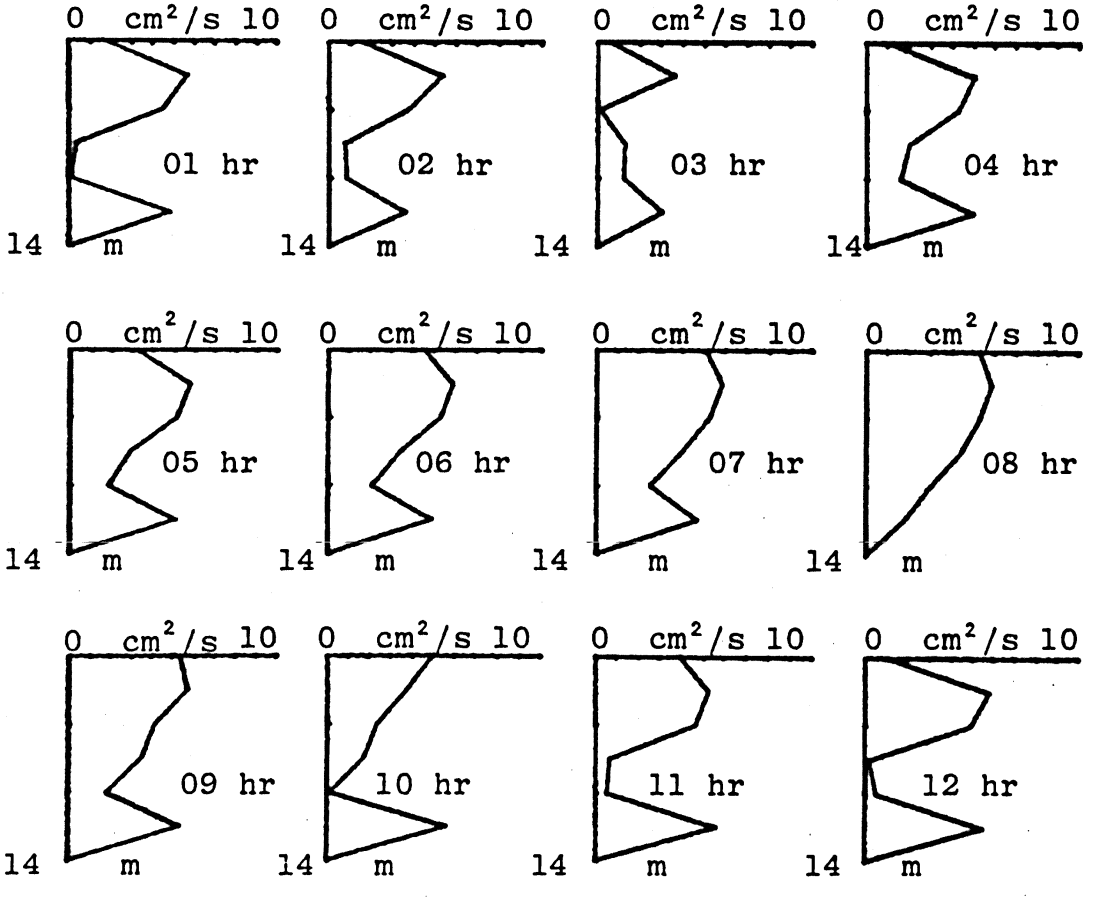

is beginning to reverse in direction giving maximum shear and a low Richardson number. The result is an uniform A_z near the A_{z_0} value implying a potential for maximum mixing as the tide is turning in the bottom layers.

The minimum in A_z throughout the tidal cycle is at the depth of maximum salinity gradient which does not substantially vary over time. The magnitude and shape of the minimum is, therefore, determined primarily by a small velocity gradient at mid-depth. The individual velocity profiles given in Figure 16 shows that there is little or no velocity gradient through the region of the A_z minimum.

The A_z Richardson number dependency coupled with the numerical hydrodynamics in a straightforward manner produces A_z variations that have been found in the field. It has not been necessary to introduce spatial functions on A_z as proposed by Blumberg (1975) to obtain known depth variations in A_z. The spatial functions appear to be required for limited formulations of the basic hydrodynamics.

PART V: SENSITIVITY ANALYSES

There are numerous properties of the model and simulation which are not illustrated by the comparisons to data. These are the time required to develop the salinity field from zero salinity conditions, the effects of changes in the vertical mixing coefficients, and the effects of wind on velocity simulations.

Initializing Salinity

One way to initialize the salinity field is to begin with a boundary salinity throughout the waterbody and let the salinity field and flow field build up together over time. The profiles of salinity at different times of such a simulation are given in Table 4. These simulations had the boundary salinity profile shown for model segment 22 and sinusoidal tide. It shows the development of salinity stratification up the estuary and the gradual movement of the salt front with time.

The time history of surface, mid-depth, and bottom salinities over time at model segment 15 about halfway up the estuary is given in Figure 20. It shows that after 20 days, the salinity is continuing to increase with time. Even after 20 days it is difficult to determine how much longer is required for there to be only tolerable change due to initialization.

The time required to initialize a salinity profile from zero initial conditions is thought to be the average residence time of the estuary based on the net non-tidal flow. For the

Figure 20. Time History of Salinity Build Up at 40 nm from Mouth of Estuary for Initiation from Zero Salinity. For Surface Layer(S), Mid-depth(M), and Bottom Layer(B)

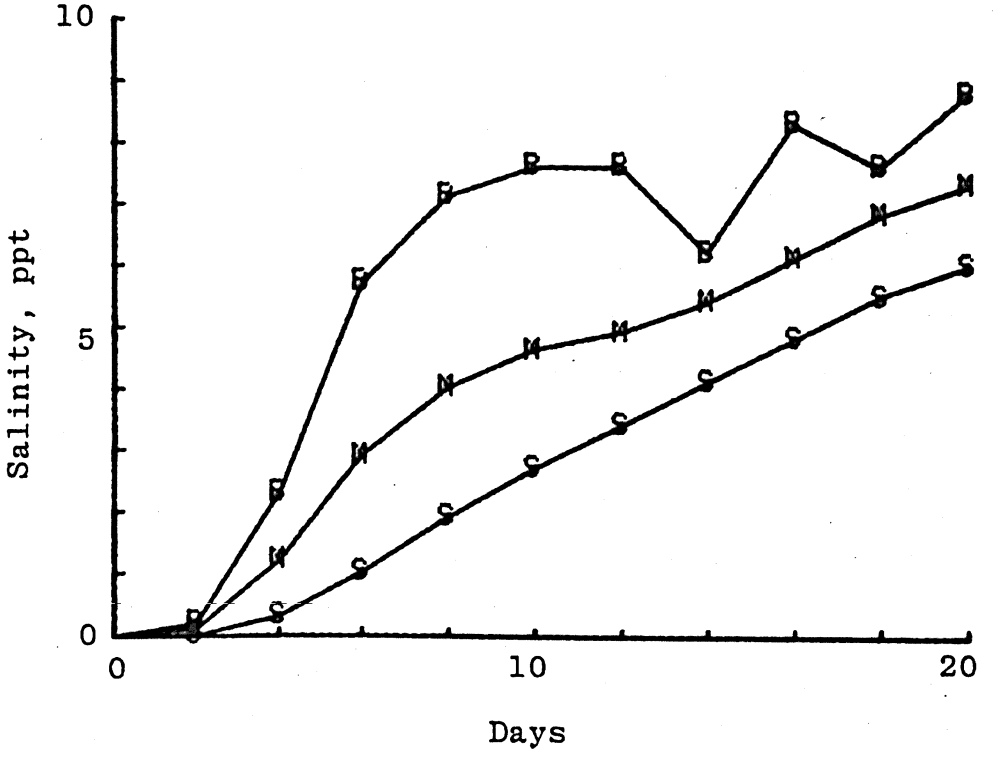

Potomac, the volume of the estuary is 7×10^9 m^3, and the net non-tidal flow based on a river flow of 50 m^3/s is 2.5×10^7 m^3/day. This suggests a residence time, hence an initialization time, of 280 days. Initialization of large waterbodies from a zero initial salinity condition is not computationally very efficient.

Sensitivity to A_z

The vertical dispersion coefficients and velocity and salinity fields are related through Equation 24. It is of interest to determine the influence of the magnitude of A_{z_0} on the velocity and salinity profiles. Simulations were made with a large A_{z_0} of 10 cm^2/s, and a low A_{z_0} of 0.6 cm^2/s. The model is nominally run with A_{z_0} of 6 cm^2/s. The simulations allow comparison of conditions over a factor of 15. The resulting tidal averaged velocity profiles for the high, low, and nominal A_{z0} are given in Figure 21 for river mile P19 and P10. It is seen that a factor of 15 in A_{z0} has little effect on the overall profile. Increasing A_{z_0} deepens the upper layer and reduces the surface velocity. For the velocity profile, a greater A_{z_0} implies greater vertical transport of momentum, hence a thickening and smoothing of the profiles. The changes in the salinity profile were insignificant. The relationships hold at P10 close to the ocean boundary as well as the P19 further upestuary.

The opposite effect is found by Wang and Kravitz (1980). Using a constant A_z with no Richardson number condition and changing it from 0.1 cm^2/s to 0.5 cm^2/s, they computed that the upper layer thickened slightly but there was an increase in

Figure 21. Variation of Velocity Profile with Vertical Dispersion Coefficient

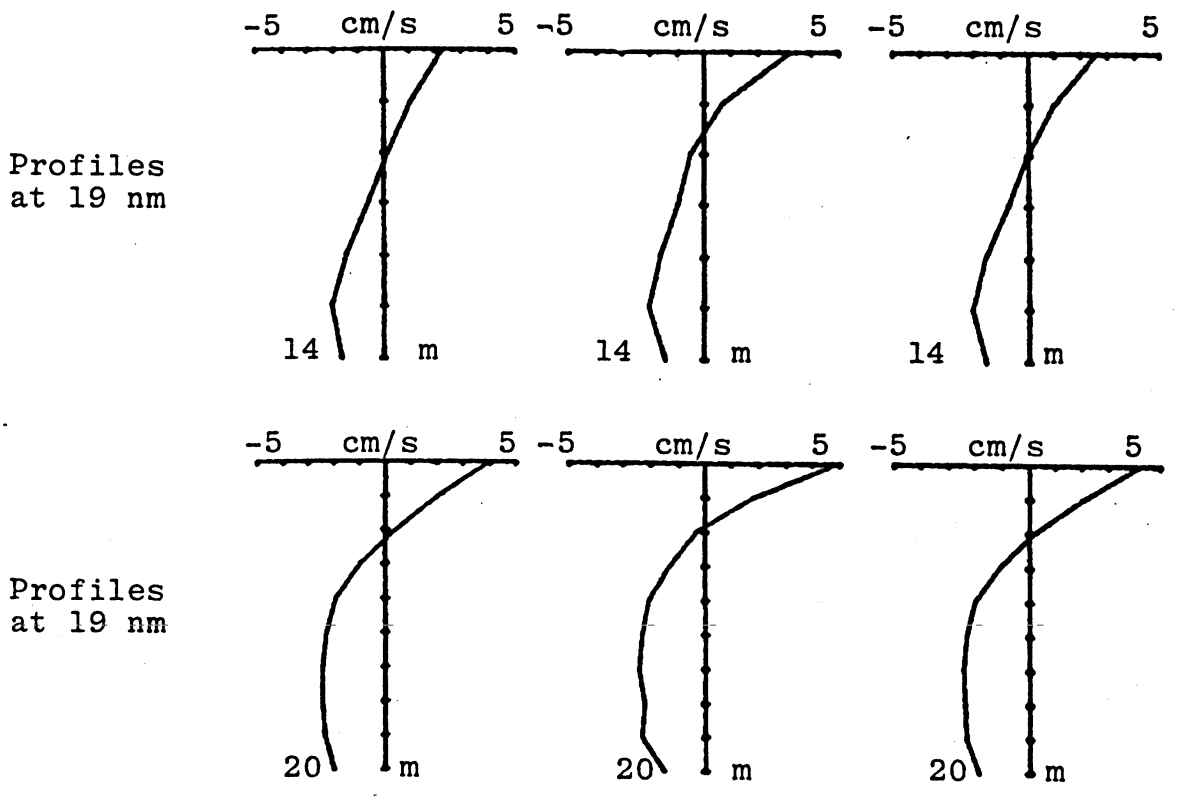

surface and lower layer velocities. They attributed this to a greater intrusion flow because of the more uniform salinity and density gradient resulting from greater mixing. The results may be erroneous because of ignoring the effects of stratification on A_z, hence overestimating it relative to the remainder of the profile, and because of increased sensitivity to changes in low values of A_{z_0} in comparison to the Pritchard (1967) estimate of 6 cm^2/s.

Effects of Wind

One important driving force for most estuaries is wind. The horizontal density gradients due to ocean salt and freshwater inflow and the solilunar tide at the mouth establish the long-term circulation with a period of two to four weeks. These forces produce the classical net circulation of bottom intrusion of salt water which mixes upward to a less saline surface outflow. On a more short-term basis Elliott (1976) has shown from the analysis of current meter data that the classical circulation pattern is disturbed by wind with a period of four or five days for the Potomac.

Two forces in the model are influenced by wind. One is the surface wind stress along the axis of the model. The second is the mean elevation at the ocean tidal boundary which must be determined from measured tidal elevations. If the surface wind stress is used independent of the boundary elevation changes and with a fixed mean elevation, the free water surface is hinged at this point. The inflow and outflow across the ocean boundary due to surface slope is then dictated by wind conditions in the

estuary alone. A fixed end condition can result in an artifical circulation within the estuary that may appear computationally correct but may not match the real conditions over the period of study.

The mean tidal elevation in the mouth of the Potomac is determined by the wind-driven surface slope of Chesapeake Bay, which in turn is often influenced by wind-driven sea level changes off Cape Henry. The Potomac is subjected to the four combinations of rising or falling mean elevation at the mouth with up- or downestuary winds. These can produce four different circulation patterns in the lower reaches of the estuary. It is necessary to have measured tide heights and concurrent winds as input data to the model to prevent the computation of artifical circulation conditions.

Within the estuary, the tendency of a surface wind is to produce a downwind surface current with a return bottom current. The return bottom current is a result of the surface elevation set up adding to the horizontal pressure gradient in the bottom layers. It is known as a barotropic response. In an estuary, the wind circulation is combined with the density circulation. A downestuary wind thus adds to the downestuary surface flow and upestuary bottom flow. An upestuary wind can produce complex circulation patterns as a result of the surface wind current opposing the surface outflow and the bottom wind current opposing the bottom inflow. By slowing down the bottom inflow, an upestuary wind can result in a three-layer flow, upestuary in the top mid-layer and downestuary in the bottom layer. These patterns

are changing from day to day due to the strength and direction of the wind and changes in boundary elevation with time, and lead to the panorama of circulation patterns found by Elliott (1976) from current meter data.

It is necessary to perform wind simulations with the model to show that it gives reasonable results. The Potomac base case simulations were made with no wind and compared to a survey period of current meter and salinity data that satisfied this condition. These comparisons were made because the detailed survey period hourly wind speed and tide height data were not available. One wind test would have been to run this period with and without wind. Another would have been to run the survey period and determine wind effects by appropriate numerical filtering similar to that used for the current meters by Pritchard and Rives (1979). Since wind data are unavailable for either of the above simulations, the tests are run for the artificial conditions of: (1) no tide with steady wind; (2) with tide with and without wind. The first case is run to eliminate the masking of water surface elevation changes due to wind by the tidal changes in order to examine the time history of the water surface set up. The second case is run to determine the contribution of wind to the circulation measured as the difference in velocity with and without the wind. Wind stress was parameterized in accordance with the well known quadratic shear stress low.

Running the model for a steady wind with no tide should result in a water surface set up in the direction of the wind with the establishment of the surface current. Countering the

surface current is a return barotropic bottom current in response to the initial water surface set up. The initial wind depresses the water surface below the final equilibrium water surface from which it rebounds due to the bottom return flow. It is a classical waterbody response to wind that has been used by Wang and Kravitz (1980) to test numerical equations of motion.

The water surface elevation over time for locations at 10, 45, and 85 nm from the mouth are shown in Figure 22 for a wind speed of 6 m/s. The 10 nm location is chosen to be near the fixed elevation boundary, the 45 nm location is in the narrow portion of the estuary, and the 75 nm location approaches the head of the estuary. The water surface response follows the classical pattern of a single depression and recovery followed by long period oscillations. The greater dip at the head of the estuary results from the fixed elevation boundary condition at the mouth. The fixed elevation boundary condition does not allow a barotropic flow to become immediately established and replace the water blown out of the upper end of the estuary. It illustrates the anomalous results that can be obtained by mismatching the boundary elevation and surface wind condition.

Simulation of the estuary with tide and wind is more realistic. It does, however, present the problem of separating wind-induced currents from the larger tidal currents. It is done here by comparing tidal averages. The base case simulations have produced the tidal average velocity profile with no wind (Figure 16). Introducing a wind after the base case has been reached allows the examination of the establishment of the wind-induced profile.

Figure 22. Wind Surface Profiles Over Time after Initiation of 6 m/s Downestuary Wind, with No Tide

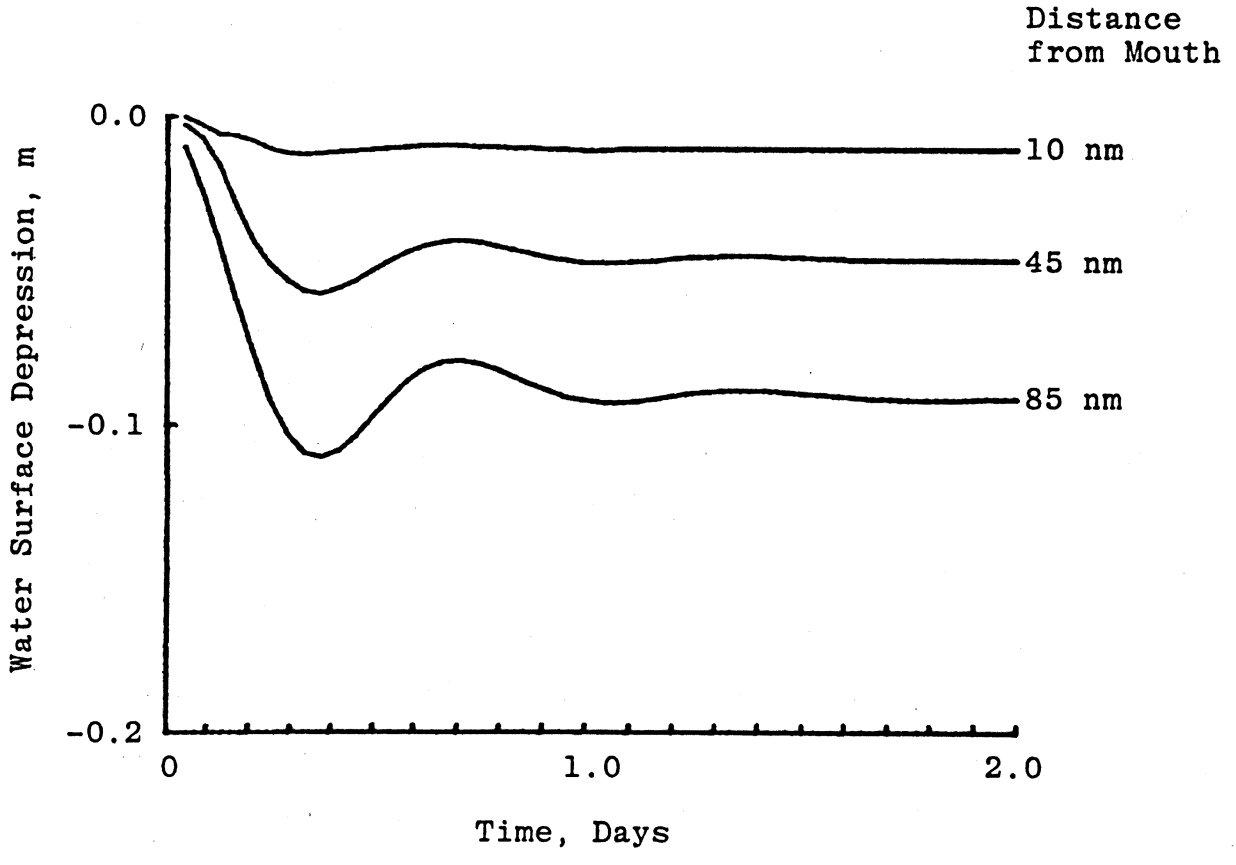

Figure 23 gives the difference in velocity with and without a downestuary wind of 1.5 m/s. The profiles are for successive tidal cycles for the survey station of 10 nm from the estuary mouth (Figure 2). Within the first cycle, a barotropic response with upestuary flow is established for the whole water column before the downestuary surface flow begins. The classical shallow surface flow in the direction of the wind with a deep bottom return is established within three tidal cycles. There is a tendency for variations in the magnitude of the barotropic flows as in the fourth and seventh tidal cycles. The initial barotropic flow in the first tidal cycle is related to the initial water surface depression shown in Figure 22, while the periodic changes in magnitude of the barotropic flow are related to the longer term dampened oscillations also shown in Figure 22.

The two wind cases illustrate the basic response of the model to wind and show that it produces expected results for known conditions. Real winds vary continuously with time although they can sustain a direction and speed for a period of days. Except for rare events, the transient wind conditions computed with the model cannot usually be found in field current meter measurements.

For an estuary as large as the Potomac, the spatial distribution of wind stress may also be important. Winds confined to the lower 30 nm of the estuary would affect circulation up estuary differently than if along the whole estuary. For the Potomac there is some evidence that there is little difference

Figure 23. Velocity with Wind Minus Velocity without Wind Averaged for Successive Tidal Periods Following Initiation of 1.5 m/s Downestuary Wind

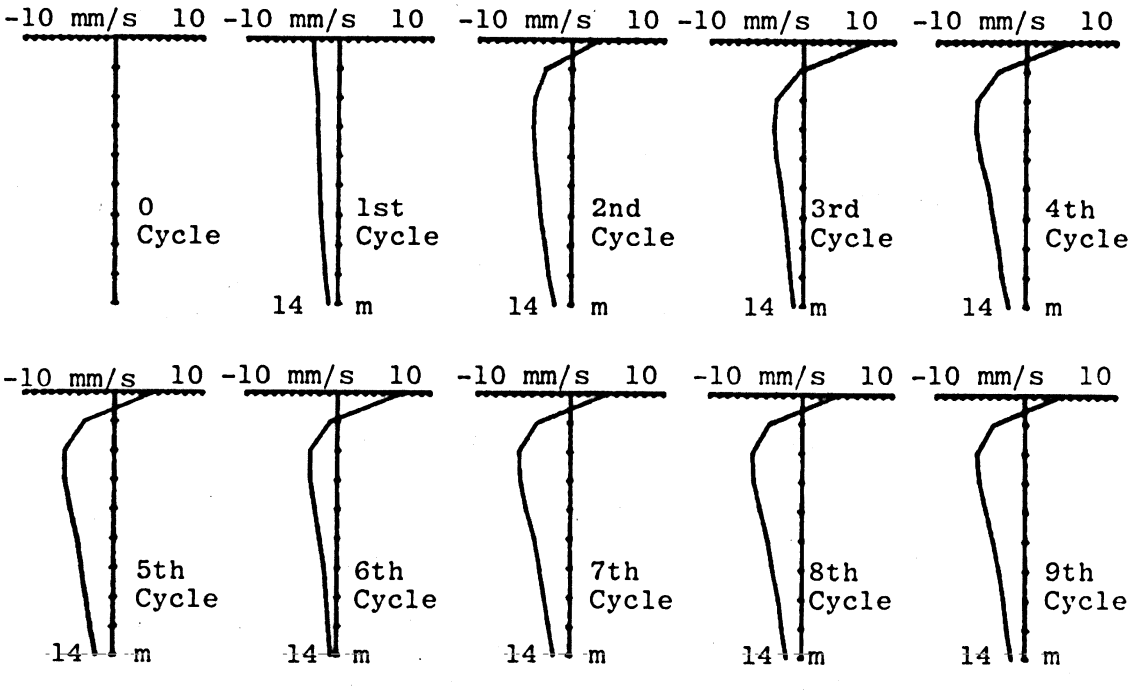

between wind conditions between Patuxent Naval Air Station and Quantico, which are near nm 19 and 60, respectively (Elliott, 1976). For winds down the estuary, however, a three-hour lag was found from the upper to the lower station, indicating that surface stress increased progressively with time and distance along the estuary rather than reaching its full magnitude at once.

Proper representation of the temporal and spatial variation of wind is a problem in input data development and formulation of surface sheer stress rather than a problem in the overall numerical hydrodynamics. The latter, however, cannot produce complete answers until the wind problem is properly formulated. The surface shear stress relationships as presently used are directly and instantaneously related to wind speed with no time lags or surface wind wave build up.

REFERENCES

Blumberg, A. F. 1975. "A Numerical Investigation into the Dynamics of Estuarine Circulation," Technical Report 91, Chesapeake Bay Institute, The Johns Hopkins University, Baltimore, Md.

Boicourt, W. A. 1980. Personal Communications, Chesapeake Bay Institute, The Johns Hopkins University, Shadyside, Md., June 1980.

Bowden, K. F. 1977. "Turbulent Processes in Estuaries," in Estuaries, Geophysics and the Environment, National Academy of Sciences, Washington, D. C., pp 46-56.

Bowden, K. F. and Hamilton, P. 1975. "Some Experiments with a Numerical Model of Circulation and Mixing in Tidal Estuary," Estuarine Coastal Mar. Sci., Vol 3, pp 281-301.

Cronin, W. B. and Pritchard, D. W. 1975. "Additional Statistics on the Dimensions of the Chesapeake Bay and its Tributaries: Cross-Section Widths and Segments per Meter Depth," Special Report 42, Chesapeake Bay Institute, The Johns Hopkins University, Baltimore, Md.

Edinger, J. E. 1974. "Feasibility of a Two Dimensional Reservoir Analysis," Report to Water Quality Section Reservoir Control, Ohio River Division, U. S. Army Corps of Engineers, Cincinnati, Ohio.

Edinger, J. E. and Buchak, E. M. 1975. "A Hydrodynamic Two-Dimensional Reservoir Model: The Computational Basis," Report to U. S. Army Engineer Division, Ohio River, Cincinnati, Ohio.

Edinger, J. E. and Buchak, E. M. 1979a. "A Hydrodynamic Two-Dimensional Reservoir Model: Development and Test Application to Sutton Reservoir Elk River, West Virginia," Report to U. S. Army Engineer Division, Ohio River, Cincinnati, Ohio.

Edinger, J. E. and Buchak, E. M. 1979b. "Preliminary LARM Simulations of the WES GRH Flume," Report to the Reservoir Water Quality Branch, Hydraulic Structures Division, Hydraulics Laboratory, U. S. Army Engineer Waterways Laboratory, Vicksburg, Miss.

Edinger, J. E. and Buchak, E. M. 1980. "Numerical Hydrodynamics of Estuaries," Estuarine and Wetland Processes, ed. P. Hamilton and K. B. Macdonald, Plenum Press, New York.

Elliott, A. J. 1976. "A Numerical Model of the Internal Circulation in a Branching Tidal Estuary," Special Report 54, Chesapeake Bay Institute, The Johns Hopkins University, Baltimore, Md.

Elliott, A. J. 1976. "A Study of the Effect of Meteorological Forcing on the Circulation in the Potomac Estuary," Special Report 56, Chesapeake Bay Institute, The Johns Hopkins University, Baltimore, Md.

Elliott, A. J. and Hendrix, T. E. 1976. "Intensive Observations of the Circulation in the Potomac Estuary," Special Report 55, Chesapeake Bay Institute, The Johns Hopkins University, Baltimore, Md.

Fischer, H. B. et al. 1979. Mixing in Inland and Coastal Waters, Academic Press, New York.

Ford, D. E. 1976. "Water Temperature Dynamics of Dimictic Lakes: Analysis and Predictions using Integral Energy Concepts," Ph.D. Thesis, University of Minnesota, Minneapolis, Minn.

Hamilton, P. 1975. "A Numerical Model of the Vertical Circulation of Tidal Estuaries and its Application to the Rotterdam Waterway," Geophs. J. R. Astr. Soc., Vol 40, pp 1-21.

Harleman, D. R. F. 1971. "One Dimensional Models," in Estuarine Modeling: An Assessment, Water Pollution Control Research Series, 16070 DZV, Office of Water Quality, Environmental Protection Agency, Washington, D. C.

Leendertse, J. J. and Liu, S-K. 1975. "A Three Dimensional Model for Estuaries and Estuaries and Coastal Seas: Volume II, Aspects of Compution," Rand Report R-1764-OWRT, Santa Monica, Calif.

Munk, W. H. and Anderson, E. R. 1948. "Note on the Thermocline," J. Mar. Res., Vol 7, pp 276-295.

Officer, C. B. 1976. Physical Oceanography of Estuaries, J. Wiley and Sons, New York.

Officer, C. B. 1977. Longitudinal Circulation and Mixing in Estuaries," in Estuaries, Geophysics and the Environment, National Academy of Sciences, Washington, D. C.

Pritchard, D. W. 1956. "The Dynamic Structure of a Coastal Plain Estuary," J. Mar. Res., Vol 15, pp 33-42.

Pritchard, D. W. 1960. "The Movement and Mixing of Contaminants in Tidal Estuaries," in Waste Disposal in the Marine Environment, Pergamon Press, New York.

Pritchard, D. W. 1967. "Observations of Circulation in Coastal Plain Estuaries," in Estuaries, Publication No. 83, AAAS, Washington, D. C., pp 37-44.

Pritchard, D. W. and Rives, S. R. 1979. "Physical Hydrography and Dispersion in a Segment of the Chesapeake Bay Adjacent to The Calvert Cliffs Nuclear Power Plant," Special Report 74, Chesapeake Bay Institute, The Johns Hopkins University, Baltimore, Md.

Rives, S. R. 1973. "A Mathematical Model of the Tide in the Potomac River," Technical Report 80, Chesapeake Bay Institute, The Johns Hopkins University, Baltimore, Md.

Wang, D-P. and Kravitz, D. W. 1980. "A Semi-Implicit Two Dimensional Model of Estuarine Circulation," J. Phys. Oceanogr., Vol 10, No. 3, pp 441-454.

Table 1

Potomac Estuary Model Widths at Indicated Model Segments*

Layer (K)	Nautical River Miles** P92			P82		P72	P66	P62	P58	P52	P42			P32		P22		P12		P02
	Estuary Widths, metres, in Indicated Model Segments (I)†																			
	2	3	4	5	6	7	8	9	10	11	12	13	14	15	16	17	18	19	20	21
2	280	690	1020	1000	1600	2760	2520	4220	4110	2370	2720	2660	5810	8300	7530	7440	6610	6620	9850	11030
3	170	330	490	610	990	1910	2160	3330	3320	1960	2040	1790	4540	7440	6630	7000	6090	6190	9040	10110
4	130	220	300	460	680	1070	1710	1750	1800	1570	1510	1340	3020	5600	5890	6480	5550	5740	8090	9060
5	60	90	230	300	520	660	1090	530	490	1100	1140	1120	1740	2350	3610	4680	4500	5000	6760	8020
6	30	20	160	150	380	430	330	120	130	580	730	910	980	230	1410	1880	3090	4220	5690	7020
7	30	20	70	60	190	210	20	50	80	250	510	730	730	20	520	640	1940	3570	4660	5910
8	20	20	10	30	120	70	20	10	20	90	260	590	600	20	130	140	1170	2900	3300	3710
9				20	100	30					140	500	460				850	2110	2230	1740
10				10	60	30					100	410	370				440	1260	1160	1040
11				10	20	20					50	330	240				150	890	180	420
12											10	250	120							

* Model Δx is 5 nautical miles and H is 2 metres.
** The numerical designation such as P92 represents a station 92 nautical miles upestuary from the estuary mouth.
† Model segments are delineated in Figure 2.

Table 2

Longitudinal Profile of Initial Salinities from Elliott (1976)

Depth m	Nautical River Miles* P92			P82		P72	P66	P62	P58	P52	P42			P32		P22		P12		P02	
	Initial Salinity, ppt, in Indicated Model Segments (I)**																				
	2	3	4	5	6	7	8	9	10	11	12	13	14	15	16	17	18	19	20	21	22
1	0	0	0	0	0.1	0.3	0.6	1.4	2.6	5.1	6.9	8.7	9.1	9.4	10.4	11.4	12.0	12.5	13.3	14.0	14.0
3	0	0	0	0	0.1	0.3	0.7	1.5	2.6	5.4	7.2	8.9	9.2	9.4	10.5	11.5	12.0	12.5	13.3	14.0	14.0
5	0	0	0	0	0.2	0.4	0.7	1.6	2.6	5.7	7.3	8.9	9.8	10.6	11.1	11.5	12.2	12.6	13.4	14.1	14.1
7	0	0	0	0	0.2	0.4	0.8	1.8	3.2	5.8	7.4	9.0	10.2	11.4	12.2	12.9	13.1	13.2	13.7	14.2	14.2
9	0	0	0	0	0.2	0.4	0.8	2.0	3.8	6.1	7.7	9.2	10.7	12.2	12.7	13.2	13.5	13.7	14.2	14.7	14.7
11	0	0	0	0.1	0.3	0.5	0.9	2.2	4.4	6.3	7.8	9.2	11.1	13.0	13.3	13.5	14.0	14.5	14.6	14.7	14.7
13	0	0	0	0.1	0.3	0.5	0.9	2.4	5.0	6.5	7.9	9.3	11.6	13.8	13.8	13.8	14.4	15.0	15.0	15.0	15.0
15				0.1	0.3	0.5					8.0	9.3	11.9				14.8	15.2	15.3	15.3	15.3
17				0.1	0.3	0.5					8.2	9.3	12.1				15.0	15.2	15.4	15.6	15.6
19				0.2	0.4	0.6					8.3	9.3	12.2				15.1	15.3	15.6	15.9	15.9
21											8.4	9.3	12.3								

* The numerical designation such as P92 represents a station 92 nautical miles upestuary from the estuary mouth.
** Model segments are delineated in Figure 2.

Table 3

Longitudinal Salinity Profile after 10-day Model Simulation to Stationary State

Layer (K)	Salinity, ppt, in Indicated Model Segments (I)*															
	2	4	6	8	9	10	11	12	13	15	17	18	19	20	21	22
2	0.1	0.8	2.0	3.5	4.4	5.2	5.9	6.9	8.0	10.1	11.4	12.0	12.6	13.1	13.6	14.2
3	0.1	0.9	2.1	3.6	4.4	5.2	6.0	7.0	8.1	10.2	11.7	12.3	12.8	13.3	13.7	14.2
4	0.1	1.0	2.1	3.6	4.4	5.4	6.4	7.3	8.3	10.3	12.0	12.7	13.2	13.6	13.9	14.2
5	0.2	1.1	2.2	3.6	4.5	5.9	6.8	7.7	8.6	10.5	12.4	13.2	13.6	13.9	14.2	14.4
6	0.2	1.2	2.2	3.6	4.8	6.5	7.3	8.2	8.8	11.0	12.9	13.7	14.0	14.4	14.7	15.4
7	0.2	1.2	2.3	3.8	5.5	7.0	7.8	8.6	9.1	11.4	13.5	14.2	14.4	14.7	15.1	15.7
8	0.2	1.3	2.3	3.8	5.7	7.4	8.2	8.9	9.3	11.5	14.0	14.5	14.7	15.0	15.5	16.1
9			2.3					9.1	9.4			14.6	14.9	15.3	15.7	16.4
10			2.3					9.3	9.5			14.9	15.1	15.4	16.0	16.7
11			2.4					9.4	9.5			15.0	15.1	15.6	16.2	17.0
12								9.4	9.5							

* Model segments are delineated in Figure 2.

Table 4

Salinity Profiles through the Estuary for Given Times after Initiation of Simulation with Zero Salinity

Elapsed Time		Nautical River Miles*									
		P97		P72		P42		P17		P02	
	Depth	Salinity, ppt, in Indicated Model Segments (I)**									
days	m	2	6	7	9	13	15	18	20	21	22
4	1	0	0	0	0	0.1	0.3	1.7	3.2	4.6	11.0
	3	0	0	0	0	0.1	0.4	3.0	5.0	6.3	12.0
	5	0	0	0	0	0.1	0.7	5.2	7.6	8.8	13.0
	7	0	0	0	0	0.2	1.2	7.7	10.3	11.3	14.0
	9	0	0	0	0	0.2	1.8	10.1	12.5	13.4	15.0
	11	0	0	0	0	0.3	1.7	12.2	14.2	15.0	16.0
	13	0	0	0	0	0.3	2.3	13.7	15.3	16.2	17.0
	15		0	0		0.3		14.7	16.3	17.3	18.0
	17		0	0		0.3		15.4	17.1	18.4	19.0
	19		0	0		0.3		15.7	17.5	19.1	20.0
	21					0.3					
10	1	0	0	0.1	0.2	1.4	2.7	5.7	7.9	9.1	11.0
	3	0	0	0.1	0.3	1.6	3.1	7.0	8.9	10.1	12.0
	5	0	0	0.1	0.3	1.8	3.8	8.8	10.4	11.3	13.0
	7	0	0	0.1	0.3	2.0	4.6	10.7	12.0	12.7	14.0
	9	0	0	0.1	0.4	2.2	5.9	12.4	13.5	14.0	15.0
	11	0	0	0.1	0.5	2.4	6.9	13.9	14.6	15.2	16.0
	13	0	0	0.1	0.6	2.6	7.6	15.0	15.6	16.2	17.0
	15		0	0.1		2.6		15.7	16.4	17.2	18.0
	17		0	0.1		2.7		16.3	17.1	18.1	19.0
	19		0	0.1		2.7		16.6	17.5	18.8	20.0
	21					2.8					
20	1	0.1	0.8	1.1	1.9	4.6	6.0	8.6	10.1	10.7	11.0
	3	0.1	0.8	1.1	2.0	4.8	6.3	9.4	10.6	11.2	12.0
	5	0.1	0.8	1.1	2.0	4.9	6.8	10.5	11.5	12.0	13.0
	7	0.1	0.8	1.1	2.1	5.1	7.3	11.7	12.5	13.0	14.0
	9	0.1	0.8	1.1	2.3	5.2	7.9	12.9	13.5	14.0	15.0
	11	0.1	0.8	1.1	2.7	5.4	8.3	13.9	14.5	15.0	16.0
	13	0.1	0.8	1.2	2.9	5.7	8.8	14.8	15.3	16.0	17.0
	15	0.1	0.8	1.1		5.7		15.4	16.1	16.8	18.0
	17		0.8	1.2		5.7		15.9	16.7	17.8	19.0
	19		0.8	1.0		5.7		16.2	17.1	18.5	20.0
	21					5.7					

* The numerical designation such as P97 represents a station 97 nautical miles upestuary from the estuary mouth.

** Model segments are delineated in Figure 2.